Geochimica et Cosmochimica Acta, Vol. 69, No. 9, pp. 2399–2418, 2005

0016-7037/05 $30.00 + .00

doi:10.1016/j.gca.2004.11.008

Hf isotope compositions and HREE variations in off-craton garnet and spinel peridotite xenoliths from central Asia

Dmitri A. Ionov,[1,2,*] Janne Blichert-Toft,[3] and Dominique Weis[2,4]

[1]Abteilung Geochemie, Max-Planck-Institut für Chemie, Postfach 3060, D-55020 Mainz, Germany
[2]Department of Earth and Environmental Sciences, Université Libre de Bruxelles, Brussels 1050, Belgium
[3]Laboratoire de Sciences de la Terre, Ecole Normale Supérieure de Lyon, 46 allèe d'Italie, 69364 Lyon, France
[4]Earth and Ocean Sciences, University of British Columbia, 6339 Stores Road, Vancouver, V6T 1Z4 Canada

(*Received May* 18, 2004; *accepted in revised form November* 1, 2004)

Abstract—Garnet-facies continental mantle is poorly understood because the vast majority of mantle xenoliths in continental basalts are spinel peridotite. Peridotite xenoliths from Vitim (southern Siberia) and Mongolia provide some of the best samples of garnet and garnet-spinel facies off-craton lithospheric mantle. Garnets in those fertile to moderately depleted lherzolites show a surprisingly broad range of HREE abundances, which poorly correlate with modal and major oxide compositions. Some garnets are zoned and have Lu-rich cores. We argue that these features indicate HREE redistribution after the partial melting, possibly related to spinel-garnet phase transition on isobaric cooling. Most peridotites from Vitim have depleted to ultra-depleted Hf isotope compositions (calculated from mineral analyses: $\varepsilon_{Hf(0)} = +17$ to $+45$). HREE-rich garnets have the most radiogenic ε_{Hf} values and plot above the mantle Hf-Nd isotope array while xenoliths with normal HREE abundances usually fall within or near the depleted end of the MORB field. Model Hf isotope ages for the normal peridotites indicate an origin by ancient partial melt extraction from primitive mantle, most likely in the Proterozoic. By contrast, an HREE-rich peridotite yields a Phanerozoic model age, possibly reflecting overprinting of the ancient partial melting record with that related to a recent enrichment in Lu. Clinopyroxene-garnet Lu-Hf isochron ages (31–84 Ma) are higher than the likely eruption age of the host volcanic rocks (~16 Ma). Garnet-controlled HREE migration during spinel-garnet and garnet-spinel phase transitions may be one explanation for extremely radiogenic $^{176}Hf/^{177}Hf$ reported for some mantle peridotites; it may also contribute to Hf isotope variations in sub-lithospheric source regions of mantle-derived magmas.

1. INTRODUCTION

The Lu-Hf isotope system has added an important new dimension to radiogenic isotope studies of mantle rocks (Blichert-Toft and Albarède, 1997; Salters and White, 1998; Vervoort and Blichert-Toft, 1999; Albarède et al., 2000; Chauvel and Blichert-Toft, 2001; Schmidberger et al., 2002; Pearson et al., 2003; Bizimis et al., 2004). The difference in compatibility between Lu and Hf in peridotite-melt systems is greater than for the Rb-Sr and Sm-Nd parent-daughter pairs (e.g., Johnson, 1998; Salters and Longhi, 1999), two other widely used radiogenic isotope systems of lithophile trace elements. This implies that a significant fractionation of the Lu/Hf ratio can occur during high degrees partial melting and therefore generate a broad range of Hf isotope variation within a given time span. Furthermore, Hf is more compatible than Sr and Nd in residual peridotites relative to melts or fluids. Hence, Hf is generally less affected by postmelting metasomatism and may better preserve isotopic signatures of early depletion. Because large-scale partial melting events are believed to play a major role in the origin of the lithospheric mantle and overlying primary crust, the Lu-Hf system may be used, in addition to the Re-Os system (Pearson et al., 2003), to establish lithospheric formation ages. That potential, however, has not yet been fully explored.

Early Hf isotope studies of mantle peridotites based on thermal-ionization mass spectrometry (TIMS) and "hot-SIMS" techniques (e.g., Salters and Zindler, 1995) outlined a broad range of Hf isotope variation in the lithospheric mantle. More recent application of multiple-collector inductively-coupled plasma mass spectrometry (MC-ICPMS) to the Lu-Hf isotope system improved data quality and reduced the amount of analytical work involved in studies of mantle samples (Blichert-Toft et al., 1997). Nevertheless, there are still very few Hf isotope data sets on mantle peridotites published in the literature (Schmidberger et al., 2002; Pearson et al., 2003; Bizimis et al., 2004). No Hf isotope data for off-craton continental mantle xenoliths have been published as yet. One of the reasons for the scarcity of Hf isotope data on mantle peridotites is the low Hf abundances in common mantle minerals (usually ≤1 ppm in clinopyroxene and garnet) and the resultant necessity to obtain and process relatively large quantities of pure mineral separates. The latter requires the use of large and well-preserved mantle samples with sufficient modal garnet and clinopyroxene.

Lu-Hf isotope studies of garnet-bearing peridotites are of particular interest because Lu has a strong affinity to garnet whereas Hf preferably enters coexisting clinopyroxene (Johnson, 1998; Salters and Longhi, 1999; Green et al., 2000; Klemme et al., 2002), thereby producing strong intermineral Lu-Hf fractionation in garnet-bearing rocks. Differences in Lu/Hf may result in broad Hf isotope differences between garnet and clinopyroxene if ambient temperature drops below

* Author to whom correspondence should be addressed (ionov@mpch-mainz.mpg.de).

Fig. 1. Locality map for xenolith and basalt occurrences (modified after Ionov, 2004).

the range, at which Hf diffusional exchange is effective. In such cases, the Lu-Hf isotope data can be used to determine cooling ages of the rocks.

Fragments of garnet-bearing mantle rocks are common as xenoliths in kimberlites in cratonic regions. By comparison, garnet-bearing peridotites are rare among xenoliths in off-craton alkali basaltic rocks, which normally only carry fragments of the shallow spinel-facies mantle (Pearson et al., 2003). Some of the currently best available samples of garnet-facies off-craton mantle worldwide are peridotite xenoliths in Miocene picritic tuff on the Vitim plateau in southern Siberia (Fig. 1) (Ashchepkov et al., 1989; Ionov et al., 1993; Ionov, 2004). The majority of peridotite xenoliths in that locality are garnet and garnet-spinel lherzolites. Many of these xenoliths are sufficiently large and fresh to enable separation of large quantities of pure garnet and clinopyroxene. Large garnet-bearing peridotite xenoliths were also found in late Cenozoic alkali basaltic fields south of Vitim: Tariat in central Mongolia and Dariganga in south-eastern Mongolia (Ionov et al., 2002; Wiechert et al., 1997).

The Vitim xenolith suite is dominated by lherzolites with high modal clinopyroxene and garnet and is one of the most fertile among well-characterized mantle xenolith suites worldwide, in stark contrast to the highly refractory mantle beneath the nearby Siberian craton (Ionov et al., 1993; Ionov, 2002). Another remarkable aspect of the Vitim xenolith suite is its generally low degree of postmelting metasomatism (Ionov et al., 1993; Ionov, 2004), compared to the widespread metasomatic alteration found in many other xenolith suites, both cratonic and off-craton (Pearson et al., 2003). Sr-Nd isotope compositions of Vitim peridotites retain signatures of ancient melting events (Ionov and Jagoutz, 1988; Ionov et al., 2005), which is rare for mantle rocks (Pearson and Nowell, 2002). It is possible, therefore, that the melt extraction record in Hf isotope compositions of the Vitim peridotites has not been significantly affected by metasomatism either. Finally, whole-rock Vitim peridotites have a broad range in heavy rare earth element (HREE) abundances, and some Vitim garnets are HREE-enriched and zoned (Ionov, 2004). These features can hardly be explained by partial melting alone and may have important effects on the Lu-Hf isotope system.

We report Hf isotope data on clinopyroxene and garnet separates from ten garnet and spinel peridotite xenoliths from the Vitim Miocene tuff (Blichert-Toft et al., 2000; Ionov and Weis, 2002). We also provide trace element compositions of garnet and pyroxenes for all samples analyzed for Hf isotopes as well as for several other garnet peridotite xenoliths from Vitim and Mongolia obtained by laser-ablation (LA) ICPMS. A major objective of this paper is to define the HREE and Hf variation ranges in minerals of off-craton mantle peridotites. Furthermore, we explore possible links between petrologic and trace element (mainly HREE and Hf) data and Hf isotope systematics in the peridotite mantle beneath Vitim and elsewhere. We pay particular attention to possible effects of spinel-garnet facies transition on the behavior of HREE and Hf, and thus on Hf isotope compositions. Finally, we seek to better establish the residence of Lu and Hf in spinel and garnet peridotites and re-assess the use of mineral analyses to obtain whole-rock Hf isotope compositions.

We show that the Vitim peridotites have a broad range of depleted $^{176}Hf/^{177}Hf$ values ($\varepsilon_{Hf(0)} = +17$ to $+43$). Those with normal, partial melting-controlled, HREE abundances plot within or near the depleted end of the mantle Hf-Nd array and largely preserve Hf isotope signatures of ancient melting events (>1 Ga), consistent with earlier results from Os, Nd and Sr isotopes. By contrast, highly radiogenic $^{176}Hf/^{177}Hf$ were found in three Vitim xenoliths that have heterogeneous and HREE-enriched garnets. We argue that HREE-enrichments (ultimately producing highly radiogenic $^{176}Hf/^{177}Hf$) in the central Asian xenoliths are caused by migration of Lu to the sites of early garnet nucleation in heterogeneous peridotite suites initially produced by different degrees of melt extraction. We further speculate that Lu fractionation during spinel-garnet phase transition in the lithospheric mantle may be an important mechanism to produce the highly radiogenic Hf isotope compositions found in mantle xenolith suites worldwide.

2. GEOLOGIC SETTING

The Vitim basaltic field is located some 200–250 km east of central Lake Baikal, in the region broadly referred to in Russian as Zabaikalie (Trans-Baikal) near the upper Vitim river (Fig. 1). The most common basement rocks are mid-Paleozoic to early Mesozoic granites. Precambrian igneous and metamorphic rocks outcrop elsewhere in the Trans-Baikal region, indicating possible existence of ancient lithosphere before the widespread intrusion of granitic magmas during and after the Caledonian orogeny (Delvaux et al., 1995; Salnikova et al., 2001).

The Vitim field is mostly made up of Pliocene-Pleistocene alkali basaltic lava flows. Xenoliths for this study come from an older picrite (or picrobasalt) tuff deposit in the eastern part of the field (Ashchepkov et al., 1989; Ionov et al., 1993; Litasov et al., 2000). K-Ar analyses of handpicked tuff groundmass have yielded Middle Miocene age estimates between 15 ± 2 and 18 ± 1 Ma (Esin et al., 1995; Ionov et al., 2005) although

Table 1. List of samples, P-T estimates and modal abundances.

Sample No.	P N&Gr	T Ca-opx	Modal composition (wt. %) Ol	Opx	Cpx	Gar	Spl	Phl	Al_2O_3 WR, %	$^{176}Hf/^{177}Hf$ analyses
Garnet peridotites:										
313-6	18.1	1063	61.6	15.9	12.6	9.9			3.73	cpx, gar
313-54	21.4	1047	59.4	14.6	13.9	12.1			4.10	cpx, gar
313-102	22.9	1053	49.9	23.0	13.6	13.5			4.76	gar
313-105	21.0	1034	63.0	16.8	11.9	8.3			3.23	cpx, gar
Garnet-spinel peridotites:										
313-110	20.5	1009	63.0	14.4	13.1	9.1	0.5	trace	3.52	cpx, gar
314-74	18.9	1026	61.1	26.6	8.8	2.8	0.7	trace	2.58	cpx
314-580	20.5	1067	64.9	16.5	11.0	7.2	0.4		3.13	cpx, (gar)
Spinel peridotites:										
314-56	/15/	889	51.0	29.9	16.6		2.5	trace	4.09	cpx
314-58	/15/	878	55.4	27.9	14.2		2.5		3.76	cpx
314-59	/18/	1027	56.8	25.4	16.0		1.8		3.23	cpx

Cpx, clinopyroxene; gar, garnet; opx, orthopyroxene; ol, olivine; spl, spinel, phl, phlogopite.
Modal compositions and P-T data are from Ionov (2004), whole-rock Al_2O_3 contents are from Ionov et al. (2005).
Equilibration pressures (P) are after Nickel & Green (1985), temperatures (T) after Brey & Köhler (1990).

precise dating of the tuff is problematic because of alteration and abundant xenolithic material. The Vitim plateau is sometimes considered as part of the Baikal rift zone (BRZ) (Glaser et al., 1999; Litasov et al., 2000). However, the basaltic field is located in a relatively flat (elevations 1000–1200 m) terrain with little tectonic activity and with no evidence for recent extension or rifting. It is distinct from the large-scale seismically active system of faults, grabens and mountain ranges some 50–100 km westwards that make up the BRZ (Sherman et al., 2004). Recent tectonic and geophysical studies (Petit et al., 1998), together with re-assessment of earlier data, indicate that the rifting in the BRZ did not significantly affect the lithospheric mantle away from the rift axis (see a review in Ionov, 2002). The Vitim volcanic field, therefore, should rather be viewed as part of the broad area of diffuse Cenozoic basaltic volcanism between the Siberian and North China cratons, which also includes the Tariat and Dariganga volcanic fields in Mongolia (Fig. 1). More information on regional geology, host volcanic rocks and xenoliths as well as relevant references are given elsewhere (Ashchepkov, 1991; Rasskazov, 1994; Esin et al., 1995; Ionov et al., 2005).

3. SAMPLE PREPARATION AND ANALYTICAL TECHNIQUES

Xenoliths ranging in size from 6 to 25 cm were cut and large portions of their interiors were crushed in a hand steel mortar. Sieved 0.3–0.6 mm size fractions of some xenoliths were separated magnetically and with heavy liquids to yield nearly pure garnet and pyroxene fractions. Most of the separates were treated ultrasonically to break mineral intergrowths and clean grain surfaces. Pure minerals for trace element and isotopic analyses were handpicked under microscope either from those separates or directly from 0.3–1.0 mm size fractions of crushed rocks. The pure separates were leached in dilute HF and HNO_3 or HCl before dissolution to remove possible contamination from grain surfaces and cracks. Mineral grains were also mounted in epoxy and polished for in situ analyses. The list of samples is given in Table 1.

Minerals were analyzed in grain mounts using a Finnigan Element-2 magnetic sector ICPMS instrument coupled with an automated UP-213 Nd-YAG laser-ablation microprobe at MPI für Chemie in Mainz. The analyses were done in low resolution mode, with ^{43}Ca as internal standard, using NIST SRM 612 glass for external calibration (Pearce et al., 1997). CaO contents in minerals were previously obtained by electron probe microbeam analysis (EPMA) (Ionov, 2004; Ionov et al., 2005). Helium was used as carrier gas and mixed with Ar downstream of the ablation cell. The laser was operated with 1 mJ/pulse energy at 10 Hz (energy density 7 j/cm^2), ablation pits were normally 120 microns in diameter. MPI-DING reference glasses (Jochum et al., 2000) were analyzed in each run for quality control. Average data obtained for komatiite glass GOR-132 and basalt glass KL2 were within 10% of preliminary reference values (except for Pb and Nb), with reproducibility of 1–4% (1 r.s.d., relative standard deviation) at ≥0.3 ppm (Table 2). Analyses of homogeneous minerals repeated in different analytical sessions (e.g., pyroxenes 313–105 and 314–56, Table 2) usually reproduced within 2–6% at >0.2 ppm and within 5–20% at 0.005 to 0.2 ppm. Overall, reliable analytical data were obtained for Sr, Y, Zr, Nb, REE, Hf, Ta, Pb, Th and U for garnet and clinopyroxene in all xenoliths; abundances of Ta, Th and U in orthopyroxene may be close to detection limits. Our results match well LA-ICPMS values obtained at another laboratory for some of the samples at >1 ppm (Ionov, 2004), but appear to be more accurate at lower levels. In particular, spurious signal components randomly generated due to instrumental problems or ablation of enriched micro-inclusions in depleted matrix can be discarded individually with a spreadsheet-based signal integration method in this study. This calculation method is time-consuming but appears to yield better results at low concentrations than software, which defines a single integration interval for all elements, without deleting individual spikes (e.g., GLITTER).

Trace elements were also determined in profiles across garnet and clinopyroxene grains in two samples by SIMS (secondary ion mass-spectrometry) on a recently upgraded Cameca 4f instrument in Montpellier generally following procedures reported by Bottazzi et al. (1994).

Table 2. LA-ICPMS analyses (in ppm) of Vitim minerals and MPI-DING reference glasses.

	GOR-132-G			KL2-G			313-6					313-54				
Sa. No.	av.8	r.s.d.	R.V.	av.7	r.s.d.	R.V.	Gar av.3	r.s.d.	Cpx av.2	r.s.d.	Opx av.3	Gar1	Gar2	Cpx av.2	r.s.d.	Opx av.2
Ti	1736	1%	1740	15182	1%	15600	1181	7%	3627	6%	1079	1092	1099	3160	1%	1078
Sr	14.4	1%	15.6	323	2%	364	0.14	2%	82.9	4%	0.36	0.14	0.16	84.0	1%	
Y	13.9	2%	12.7	24.6	1%	26.8	26.5	4%	3.8	13%	0.28	26.4	29.1	3.4	6%	0.31
Zr	10.2	2%	10.3	142	1%	159	30.3	2%	27.8	9%	1.57	23.7	26.9	20.8	0%	1.30
Nb	0.065	6%	0.071	13.8	2%	15.8	0.09	15%	0.81	0%	0.046	0.064	0.13	0.77	1%	0.06
La	0.09	2%	0.085	13.1	2%	13.2	0.007	14%	1.30	4%	0.003	0.008	0.009	1.54	3%	0.007
Ce	0.39	5%	0.38	29.9	3%	32.9	0.07	6%	4.19	3%	0.023	0.078	0.088	4.36	2%	0.028
Pr	0.08	3%	0.095	4.37	2%	4.71	0.03	9%	0.77	2%	0.006	0.030	0.037	0.78	0.5%	0.006
Nd	0.70	2%	0.71	21.4	2%	21.7	0.41	12%	4.67	1%	0.037	0.41	0.45	4.57	0%	0.04
Sm	0.52	3%	0.52	5.53	2%	5.55	0.61	5%	1.59	0%	0.025	0.62	0.57	1.53	2%	0.02
Eu	0.25	2%	0.26	1.85	2%	1.95	0.39	3%	0.54	2%	0.011	0.38	0.38	0.52	1%	0.012
Gd	1.27	3%	1.26	5.83	1%	6.10	2.08	3%	1.69	1%	0.043	1.96	1.95	1.56	0%	0.044
Tb	0.28	2%	0.28	0.87	2%	0.93	0.52	5%	0.22	5%	0.008	0.51	0.53	0.20	2%	0.009
Dy	2.35	3%	2.14	5.34	2%	5.35	4.40	6%	1.11	7%	0.055	4.35	4.87	1.01	3%	0.059
Ho	0.55	3%	0.53	0.99	1%	0.99	1.03	10%	0.16	12%	0.011	1.00	1.23	0.14	4%	0.011
Er	1.69	3%	1.62	2.55	2%	2.64	3.01	10%	0.30	19%	0.027	2.92	3.86	0.27	5%	0.028
Tm	0.26	3%	0.244	0.34	2%	0.34	0.43	8%	0.033	21%	0.003	0.44	0.55	0.03	2%	0.005
Yb	1.76	3%	1.61	2.14	3%	2.13	2.78	5%	0.17	29%	0.026	2.90	3.78	0.14	8%	0.032
Lu	0.26	3%	0.24	0.30	2%	0.296	0.39	4%	0.018	21%	0.003	0.41	0.54	0.017	1%	0.005
Hf	0.38	3%	0.37	3.90	1%	4.14	0.49	18%	1.10	10%	0.057	0.41	0.45	0.93	3%	0.045
Ta	0.03	7%	0.034	0.96	2%	0.97	0.002	35%	0.047	2%	0.0008	0.001	0.002	0.033	7%	0.0003
Pb	17.3	4%	21	1.57	4%	2.20	0.005	73%	0.07	53%	0.002	0.001	0.003	0.077	10%	0.004
Th	0.007	13%	0.016	1.02	1%	1.03	0.004	32%	0.073	22%	0.0003	0.003	0.004	0.088	10%	0.001
U	0.04	6%	0.045	0.53	3%	0.55	0.005	8%	0.015	9%	0.0005	0.005	0.009	0.018	15%	0.001
Lu/Hf							0.79		0.02		0.06	1.00	1.20	0.02		0.11
Sa.No.							313-6					313-54				
% Hf							25%		71%		5%	27%		70%		4%
WR Hf, ppm (calculated / measured)							0.196 / 0.204					0.189 / 0.216				
WR Lu, ppm (calculated / measured)							0.041 / 0.050					0.061 / 0.065				

Reference values (R.V.) for MPI-DING glasses are from Jochum et al. (2000). R.s.d., relative standard deviation per cent (one sigma divided by average). B.d., below detection; n.d., not determined.

%Hf is the proportion of Hf (wt. %) contained in a given mineral relative to total Hf calculated for whole-rock peridotite from mineral analyses and modal abundances.

Measured whole-rock Lu and Hf are from Ionov (2004) and Ionov et al. (2005).

Hf isotope analyses were done at Ecole Normale Supérieure de Lyon (ENSL) and Université Libre de Bruxelles (ULB). Chemical separation of Lu (ENSL only) and Hf at both laboratories was carried out following the protocol of Blichert-Toft (2001). Samples analyzed at ULB were not spiked and thus used only to determine $^{176}Hf/^{177}Hf$. Mineral separates were attacked in steel-jacketed Teflon bombs at 160°C with a mixed ^{176}Lu-^{180}Hf spike (ENSL only) added to the samples from the outset of the dissolution procedure. Upon complete sample-spike homogenization, a Hf-bearing fraction was separated from a REE-bearing fraction on a cation-exchange column. A combined Yb-Lu fraction was subsequently isolated from the latter on an HDEHP column (ENSL only), while Hf was further purified, first through an anion-exchange column to remove remaining matrix elements, then through a cation-exchange column serving to separate Ti and some Zr from the Hf. Only double-distilled reagents and new resins were used throughout the dissolution and elution procedures. Total procedural Lu and Hf blanks were <20 pg and <25 pg, respectively, which are low enough for even the most depleted of the samples to be blank-insensitive.

The isotope analyses were carried out on MC-ICPMS instruments: "VG Plasma P54" at ENSL and "Nu Plasma" at ULB, following the analytical procedure of Blichert-Toft et al. (1997). All measured Hf isotope ratios were corrected for W and Ta, and Lu and Yb interferences at masses 180 and 176, respectively, by monitoring the isotopes ^{182}W, ^{181}Ta, ^{175}Lu, and ^{173}Yb, and normalized for mass fractionation to $^{179}Hf/^{177}Hf$ of 0.7325 using an exponential law. During the period of data collection, the JMC-475 Hf standard at ENSL gave an unweighted mean for $^{176}Hf/^{177}Hf$ of 0.282160 ± 0.000010 (2σ) with the standard run alternately with samples to constantly monitor machine performance. 16 analyses of the JMC-475 at ULB on the day when samples for this paper were measured gave an unweighted mean for $^{176}Hf/^{177}Hf$ of 0.282155 ± 0.000013 (2 σ); the overall mean value for the JMC475 at ULB for 2002 (356 analyses) is 0.282157 ± 0.000017 (2 σ). Signal intensities for the samples were 35%–100% of those for the standard (250 ppb Hf).

4. ROCK TYPES, MAJOR ELEMENT COMPOSITIONS AND P-T ESTIMATES

A list of samples analyzed for Hf isotopes is given in Table 1 together with pressure, temperature and modal estimates. The Vitim xenoliths are medium- to coarse-grained, their textures can be broadly defined as protogranular (Fig. 2a). Three xenoliths from this study contain rare accessory phlogopite (Table 1). Ionov et al. (1993) and Ionov (2004) identified three major rock types: spinel, garnet-spinel and garnet peridotites. The garnet lherzolites contain 8–13 wt.% of garnet, 12–14 wt.% of clinopyroxene and no interstitial spinel. Garnet grains range from equant (Fig. 2c) to highly irregular (Fig. 2a) and may contain inclusions of olivine, pyroxenes and rare spinel. Garnet may be heterogeneously distributed on a cm-scale while proportions of olivine and

Table 2. (Continued)

313-105								313-110			
Gar1	Gar2	Gar av.6	r.s.d.	Cpx av.6	r.s.d.	Opx av.6	r.s.d.	Gar 1	Gar2	Gar av.4	r.s.d.
1116	n.d.	1233	13%	3255	2%	1082	2%	830	827	813	2%
0.14	0.16	0.14	15%	79.2	2%	0.47	8%	0.08	0.09	0.09	9%
25.8	40.6	31.7	17%	4.64	4%	0.39	7%	72.1	79.8	77.7	7%
23.5	27.7	25.6	6%	22.3	3%	1.51	6%	26.4	22.6	25.3	7%
0.048	0.077	0.060	39%	0.47	7%	0.036	14%	0.024	0.029	0.022	24%
0.006	0.008	0.007	21%	1.00	2%	0.005	17%	0.005	0.004	0.003	27%
0.063	0.079	0.070	20%	3.43	2%	0.023	11%	0.038	0.042	0.036	13%
0.027	0.037	0.031	15%	0.71	3%	0.007	4%	0.019	0.023	0.019	15%
0.36	0.49	0.43	14%	4.49	3%	0.045	10%	0.29	0.32	0.28	8%
0.60	0.64	0.65	5%	1.58	3%	0.029	23%	0.50	0.52	0.51	2%
0.38	0.39	0.40	3%	0.55	4%	0.013	14%	0.38	0.36	0.37	3%
2.00	2.41	2.22	7%	1.78	4%	0.053	14%	2.37	2.17	2.41	8%
0.51	0.66	0.58	9%	0.25	4%	0.010	8%	0.76	0.75	0.79	6%
4.28	6.24	5.06	14%	1.25	3%	0.077	6%	8.54	8.98	9.08	6%
0.96	1.59	1.21	18%	0.19	5%	0.014	8%	2.64	2.95	2.86	6%
2.83	4.99	3.69	20%	0.40	6%	0.037	37%	10.2	12.0	11.2	8%
0.42	0.76	0.55	22%	0.043	6%	0.006	12%	1.83	2.24	2.05	9%
2.80	5.30	3.89	22%	0.23	8%	0.041	11%	14.7	18.2	16.5	11%
0.41	0.80	0.58	23%	0.027	10%	0.006	18%	2.54	3.23	2.85	13%
0.44	0.48	0.46	8%	1.01	2%	0.056	13%	0.35	0.34	0.35	3%
0.001	0.003	0.002	66%	0.045	4%	0.001	43%	b.d.	b.d.	b.d.	
0.004	0.027	0.019	65%	0.041	40%	0.027	95%	0.004	0.011	0.007	45%
0.000	0.003	0.001	77%	0.024	10%	0.0002	90%	0.001	0.001	0.001	29%
0.002	0.002	0.002	24%	0.006	15%	0.0006	102%	0.001	0.002	0.001	14%
		1.27		0.03		0.11				8.1	
		313-105								313-110	
		23%		72%		6%				21%	
		0.167 / 0.198								0.155 / 0.205	
		0.053 / 0.055								0.26 / 0.10	

pyroxenes remain nearly constant (Fig. 2). Garnet-spinel peridotites differ from garnet peridotites primarily by common presence of interstitial spinel. Furthermore, abundances and textural relationships of garnet and spinel vary broadly both within individual xenoliths and sample-to-sample. In garnet-poor xenoliths, garnet normally mantles spinel and rarely forms equant grains (Fig. 2b). In garnet-rich xenoliths, spinel normally occurs inside garnet (Fig. 2d) and may be locally absent (Fig. 2c). No samples in this study contain veins or clearly defined domains with distinct modal compositions. The petrographic and chemical data indicate that garnets in many Vitim xenoliths grew at the expense of spinel and pyroxenes (most likely owing to a decrease in temperature) as a result of the reaction (Ionov et al., 1993; Glaser et al., 1999):

$$\mathrm{Sp} + \mathrm{En} + \mathrm{Di} \leftrightarrows \mathrm{Fo} + \mathrm{Gross} + \mathrm{Py} \quad (1)$$

Garnets commonly have kelyphite material at their rims and inside cracks (Fig. 2). The kelyphite rims typically consist of an inner amorphous or crypto-crystalline layer and an outer fine- to medium-grained layer made up mainly of orthopyroxene and spinel (Figs. 2d and 2h in Ionov, 2004). The outer layer may form due to a reversal of the garnet-building reaction (1) because of isobaric heating in the mantle some time before the eruption; the inner layer apparently formed due to abrupt heating of xenoliths by the host magma and a pressure drop during uplift to the earth's surface (Ionov et al., 1993; Glaser et al., 1999; Ionov, 2004).

Spinel peridotites are subdivided in two types. The first type (SP-1, samples 314–56 and –59) has protogranular microstructure with anhedral and unstrained minerals, common spinel-pyroxene intergrowths and no preferred mineral orientation. These rocks typically have low equilibration temperatures and high modal clinopyroxene (Table 1). The second type (SP-2, sample 314–59) has fabrics similar to that of garnet-free domains in the garnet-spinel peridotites, in particular prismatic olivine grains with slight to moderate preferred orientation (Kern et al., 1996).

The majority of Vitim peridotites are fertile to moderately depleted in terms of their modal and major element compositions (Ionov, 2004; Ionov et al., 2005). Whole-rock Al_2O_3 in xenoliths from this study ranges from 2.6 to 4.8 wt.%, with >3.1 wt.% in nine samples out of ten (Table 1). Consistent with fertile modal and whole-rock compositions, the silicate minerals have low Mg# (0.885–0.905 in olivine; Ionov, 2004); garnet is low in chromium (0.9–1.4 wt.% Cr_2O_3 in cores). Pyroxenes are commonly zoned with respect to Al, Cr and Ca, probably due to incomplete equilibration following garnet formation or in response to late-stage heating. Cr_2O_3 contents in garnet rims are higher by 0.2–0.4 wt.% than in the cores whereas the contents of other elements do not change along grain profiles.

Temperature (T) estimates from the Ca-opx thermometer (Brey and Köhler, 1990) for mineral cores in garnet-bearing peridotites from this study range from 1000 to 1060°C; pressures (P) (Nickel and Green, 1985) range from 18 to 23 kbar (Table 1). The T value for spinel peridotite 314–59 (1012°C), as well as many other SP-2 spinel peridotites (Ionov, 2004) falls within the range for the garnet-bearing xenoliths. Assuming that temperature gradually increases with depth, garnet-spinel, spinel and garnet peridotites appear to coexist in the depth range ~60–75 km (18–23 kbar), most likely because the spinel-garnet phase transition takes place at greater depths for more refractory peridotites (Nickel and Green, 1985; Robinson

Table 2. (Continued)

	313-110			314-74							314-580				
Sa. No.	Cpx av.2	r.s.d.	Opx av.2	Gar 1	Gar2	Gar av.5	r.s.d.	Cpx av.2	r.s.d.	Opx av.2	Gar av.3	r.s.d.	Cpx av.2	r.s.d.	Opx
Ti	2823	0%	838	1174	1134	1168	4%	1558	11%	519	1020	8%	3249	3%	1009
Sr	70.5	1%	0.21	0.17	/0,9/			60.4	11%	0.25	0.17	30%	98.4	2%	0.53
Y	3.21	0%	0.23	17.5	29.6	22.5	15%	7.5	9%	0.73	22.4	12%	4.0	4%	0.38
Zr	19.6	1%	1.02	23.5	50.1	34.2	24%	12.3	23%	1.34	30.4	28%	37.9	15%	3.05
Nb	0.22	3%	0.016	0.13	0.25	0.20	24%	0.52	27%	0.028	0.125	66%	1.19	5%	0.089
La	0.80	0%	0.002	0.012	0.04			1.11	23%	0.005	0.012	37%	2.19	2%	0.010
Ce	2.76	2%	0.010	0.145	0.20	0.176	5%	2.94	27%	0.022	0.135	44%	6.94	6%	0.048
Pr	0.56	0%	0.003	0.058	0.08	0.065	3%	0.50	22%	0.005	0.055	39%	1.22	7%	0.011
Nd	3.64	4%	0.027	0.64	0.96	0.78	8%	2.85	21%	0.039	0.67	39%	6.75	9%	0.070
Sm	1.39	2%	0.016	0.69	0.98	0.82	8%	0.97	13%	0.026	0.74	23%	2.00	6%	0.050
Eu	0.48	3%	0.008	0.39	0.54	0.46	10%	0.38	11%	0.011	0.42	20%	0.65	9%	0.017
Gd	1.54	5%	0.034	1.86	3.24	2.38	6%	1.39	10%	0.052	2.51	21%	1.96	6%	0.068
Tb	0.20	2%	0.007	0.41	0.73	0.54	8%	0.23	8%	0.012	0.56	13%	0.25	4%	0.012
Dy	0.98	3%	0.046	3.30	5.71	4.24	9%	1.54	7%	0.106	4.40	11%	1.20	5%	0.084
Ho	0.14	6%	0.008	0.66	1.29	0.92	14%	0.30	9%	0.027	0.92	13%	0.16	4%	0.015
Er	0.26	4%	0.024	1.69	3.43	2.47	20%	0.76	12%	0.091	2.40	14%	0.32	3%	0.040
Tm	0.026	1%	0.004	0.23	0.51	0.36	23%	0.10	16%	0.015	0.32	16%	0.03	2%	0.004
Yb	0.12	3%	0.020	1.47	3.30	2.28	26%	0.59	16%	0.121	1.94	17%	0.16	3%	0.038
Lu	0.013	1%	0.003	0.18	0.49	0.31	33%	0.079	21%	0.019	0.25	20%	0.017	6%	0.005
Hf	0.89	1%	0.043	0.33	0.73	0.48	16%	0.50	10%	0.040	0.44	28%	1.25	16%	0.094
Ta	0.017	8%	0.001	0.006	0.012	0.007	22%	0.059	67%	0.003	0.008	73%	0.181	19%	0.006
Pb	0.11	7%	0.004	0.004	0.006	0.007	48%	0.034	12%	0.005	0.005	49%	0.046	20%	0.006
Th	0.022	1%	0.0004	0.004	0.008	0.006	10%	0.053	39%	0.0034	0.004	44%	0.110	6%	0.0009
U	0.006	12%	0.0003	0.007	0.011	0.009	5%	0.011	14%	0.0004	0.007	53%	0.021	9%	0.0008
Lu/Hf	0.02		0.06			0.65		0.16		0.47	0.57		0.01		0.05
Sa.No.	313-110					314-74					314-580				
% Hf	75%		4%			20%		65%		16%	17%		74%		8%
WR Hf						0.069 / 0.116					0.185/ n.d.				
WR Lu						0.021 / 0.030					0.021				

and Wood, 1998; Walter, 2003). In particular, the garnet-spinel and high-T spinel peridotites have higher Cr_2O_3/Al_2O_3 (0.12–0.16) than garnet lherzolites (0.08–0.11) (Ionov, 2004).

5. RESULTS

5.1. Trace-Element Compositions of Minerals

Table 2 gives average trace element abundances and r.s.d. values for minerals in Vitim xenoliths analyzed for Hf isotopes. Individual analyses of garnets with the lowest (gar1) and highest (gar2) HREE are provided for those samples, in which garnet was found to be heterogeneous.

Primitive mantle (PM)-normalized REE patterns of garnet and pyroxenes are fairly smooth, with downward slopes from MREE to less compatible LREE (Fig. 3). Clinopyroxene 314-580 has $La/Nd_{PM} < 1$, like the other samples, but its MREE-LREE levels are distinctly higher, possibly due to metasomatism. The HREE-MREE patterns in clinopyroxene from spinel lherzolites (Fig. 3a) are nearly flat while the REE_{PM} values in clinopyroxene from the garnet-bearing rocks (Fig. 3b) decrease smoothly from Eu to Lu, consistent with increasing affinity of heavier REE to garnet (Hauri et al., 1994; Johnson, 1998; Salters and Longhi, 1999). Clinopyroxene REE patterns in all garnet-bearing xenoliths are similar, in particular for MREE, with somewhat more scatter for LREE and HREE (Fig. 3b). Clinopyroxene in garnet-poor xenolith 314-74 has the highest HREE and lowest MREE.

Similar to pyroxene compositions, the MREE in Vitim garnets show little variation. By contrast, their HREE patterns fan out from Tb to Lu, with a broad variation range for Lu (0.2–3.2 ppm) (Fig. 3c). Garnets in many Vitim xenoliths have higher Lu and Yb abundances than those estimated for garnet in primitive mantle at appropriate P-T conditions (Fig. 4a). These estimates assume that nearly all whole-rock Lu (0.064 ppm in primitive mantle after Hofmann, 1988 or 0.074 ppm after Sun and McDonough, 1989) is hosted by 10–13 wt.% of garnet (typical modes for fertile Vitim rocks), yielding a range of 0.5–0.75 ppm Lu for garnet (see discussion below).

Clinopyroxenes from garnet and spinel peridotites usually have minor negative Hf anomalies ($Hf/Sm_{PM} < 1$) (Figs. 3 and 5). By comparison, all orthopyroxenes have marked positive Hf anomalies ($Hf/Sm_{PM} >> 1$). Hf/Sm_{PM} in garnets range from slightly below to slightly higher than unity (Figs. 3c-d and 5).

Garnets in Mongolian xenoliths (electronic annex; Fig. 4b) fall in the same Lu-Yb abundance range as the Vitim garnets; some are rich in Lu (≥1 ppm). Comparisons with scarce published data on garnet from other basalt-hosted fertile peridotite xenoliths (Fig. 4b) further show that HREE-rich garnets are not unique to the Vitim suite. Stern et al. (1999) found 2–4 ppm Lu in garnet from two Pali-Aike xenoliths (Patagonia); the latter value exceeds the highest Lu measured in Vitim garnets. Kempton et al. (1999) reported a range of 0.4–1 ppm Lu in garnet from another five Pali-Aike xenoliths. Garnet in xenoliths from Mingxi in eastern China was found to contain 0.6–1.1 ppm Lu, i.e., within the range of the majority of the Vitim garnets. Even higher Lu and Yb abundances (0.8–2.3 ppm Lu) were reported for garnets from Nushan in SE China (Xu et al., 2003). However, the Nushan xenoliths, typically low in garnet (0.1 wt.%) and strongly metasomatized (Xu et al., 2000), appear to be shallow, garnet-spinel facies rocks rather than true garnet lherzolites.

Ionov (2004) showed that HREE abundances increase two-fold from rim to core in garnet 313-102, but remain nearly constant in a profile across garnet 313-54. Because the zoning

Table 2. (Continued)

314-56						314-58			314-59		
Cpx av.6	r.s.d.	Opx av.5	r.s.d.	Ol av.2	r.s.d.	Cpx av.2	r.s.d.	Opx av.2	Cpx av.2	r.s.d.	Opx av.2
3816	3%	806	13%	n.d.		3795	0%	718	2391	0%	728
83.9	6%	0.09	19%	0.011	58%	72.3	1%	0.13	65.3	1%	0.23
23.0	4%	0.87	5%	0.020	19%	21.8	7%	0.71	14.4	1%	0.96
39.5	3%	1.40	4%	0.012	3%	34.8	6%	1.16	24.4	0%	1.75
0.17	5%	0.004	37%	0.0011	22%	0.12	2%	0.003	0.48	0%	0.029
1.10	5%	0.001	91%	0.0007	63%	0.81	3%	0.002	1.03	2%	0.003
3.82	4%	0.005	55%	0.0015	77%	3.20	0%	0.006	3.18	1%	0.016
0.77	5%	0.002	50%	0.0005	51%	0.69	2%	0.001	0.60	1%	0.004
4.94	4%	0.012	25%	0.0013	82%	4.54	2%	0.013	3.72	2%	0.030
1.98	4%	0.012	26%	0.0038	3%	1.89	1%	0.010	1.40	3%	0.021
0.79	3%	0.007	15%	0.0004	37%	0.77	3%	0.006	0.54	2%	0.012
3.02	4%	0.032	15%	0.0017	30%	2.93	4%	0.031	2.05	0%	0.049
0.55	2%	0.010	13%	0.0002	33%	0.54	5%	0.008	0.37	1%	0.013
4.06	2%	0.096	4%	0.0022	106%	3.98	6%	0.084	2.68	1%	0.123
0.87	2%	0.028	3%	0.0008	1%	0.86	6%	0.027	0.57	2%	0.035
2.55	2%	0.126	5%	0.0023	8%	2.48	9%	0.112	1.66	1%	0.134
0.37	2%	0.027	10%	0.0011	20%	0.36	6%	0.023	0.24	1%	0.027
2.53	3%	0.245	8%	0.011	13%	2.43	5%	0.214	1.58	1%	0.222
0.37	2%	0.048	8%	0.0033	9%	0.35	6%	0.042	0.23	1%	0.041
1.24	3%	0.049	8%	0.0008	6%	1.11	5%	0.041	0.83	3%	0.051
0.017	13%	b.d.		0.0002	132%	0.011	15%	0.000	0.023	1%	0.001
0.082	32%	0.029	82%	0.030	7%	0.055	13%	0.005	0.067	17%	0.004
0.014	9%	0.0002	101%	0.0001	12%	0.026	92%	0.0002	0.059	20%	0.0004
0.006	11%	0.0001	129%	0.0001	213%	0.005	3%	0.0001	0.012	1%	0.0002
0.30		0.98		4.1		0.31		1.04	0.27		0.80
314-56						314-58			314-59		
93%		7%		0.2%		93%		7%	91%		9%
0.22 / 0.27						0.169 / 0.195			0.146 / 0.189		
0.077 / 0.071						0.061 / 0.082			0.047 / 0.050		

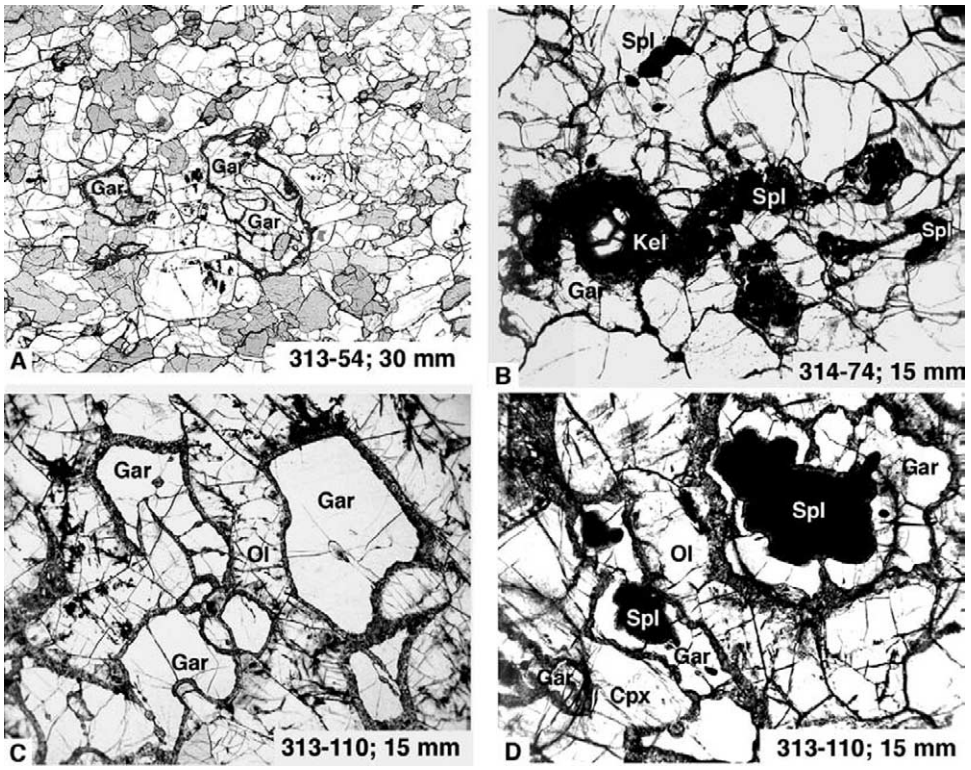

Fig. 2. (a–d) Photomicrographs of Vitim peridotite xenoliths in plane-polarized transmitted light. Sample numbers and the field of view along the long axis are indicated on each photograph. Ol, olivine; Cpx, clinopyroxene; Gar, garnet; Spl, spinel, Kel, kelyphite (garnet breakdown products, commonly dark due to alteration). (a) Coarse, protogranular garnet lherzolite with complex, irregularly shaped garnet. Dark spots inside olivine and at some grain boundaries are due to secondary alteration. (b) Garnet-poor (small grains only) garnet-spinel lherzolite. Spinel is locally mantled with garnet and kelyphite. (c) Garnet-rich zone in garnet-spinel lherzolite with large, equant, mainly inclusion-free garnet grains (rimmed with granular kelyphite). (d) Garnet-mantled spinel in another portion of the same sample as in (c).

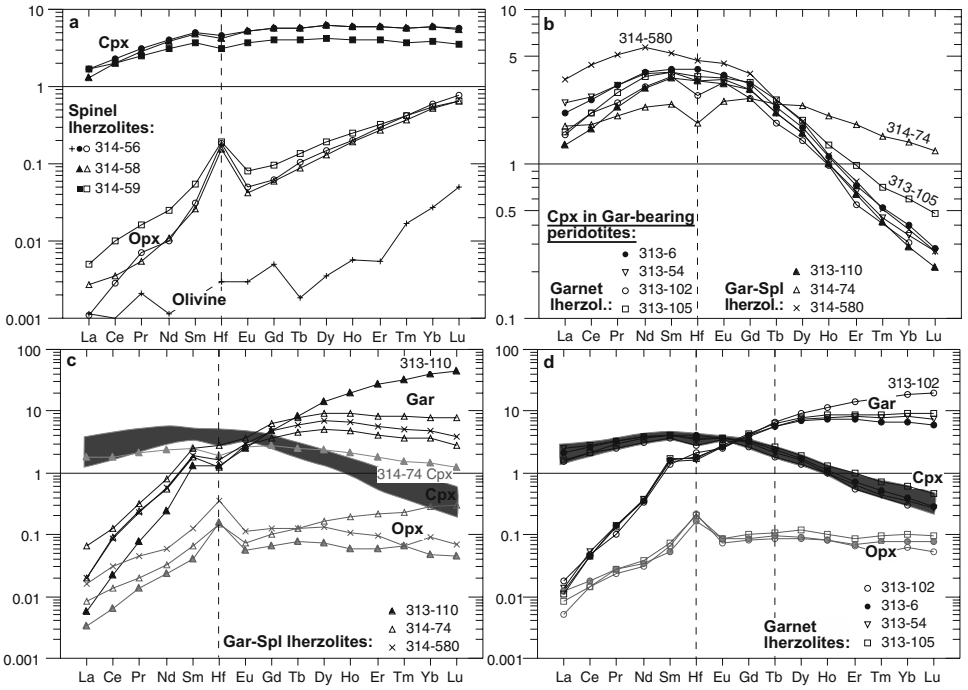

Fig. 3. Primitive mantle-normalized (Hofmann, 1988) REE and Hf abundances in garnet and pyroxenes from xenoliths analyzed for Hf isotopes. Olivine is also shown for spinel lherzolite 314-56.

was only found in a single grain from one xenolith, it remained unclear if such zoning is typical of Vitim garnets. This study clearly demonstrates that significant core-rim zoning and grain-to-grain HREE variations are common in garnet from Vitim and Mongolian peridotite xenoliths. For example, Lu abundances in cores of individual grains may differ from each other more than two-fold (0.4–0.8 ppm in 313-105; 0.18–0.49 ppm in 314-74); r.s.d. values for average garnet compositions in those xenoliths gradually increase from 2–5% for Sm and Eu to 20–35% for Yb and Lu (Table 2). New SIMS grain profiles in

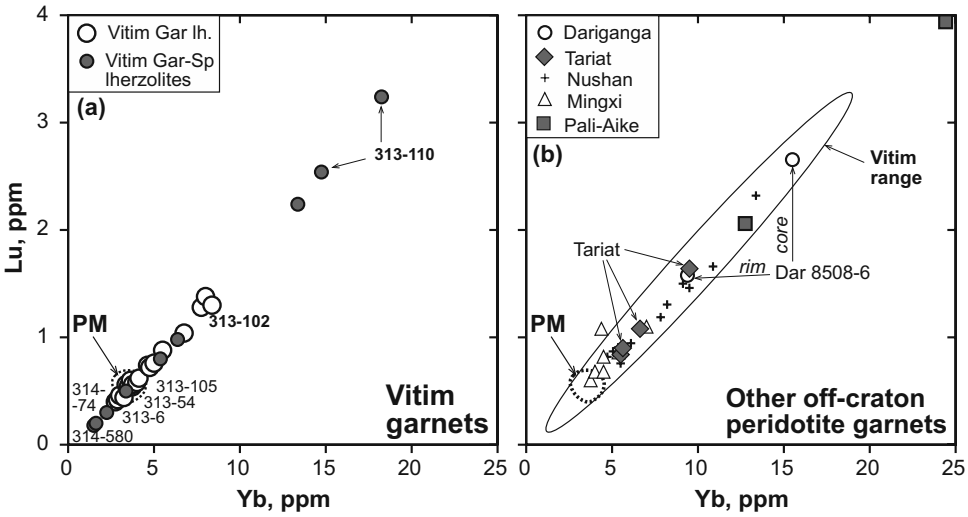

Fig. 4. Lu-Yb co-variation diagrams for garnet in peridotite xenoliths from Vitim (a) and other off-craton xenolith suites (b). Analyses with highest and lowest Lu and Yb are shown separately for each sample if Lu abundances differ by >20%; average values are shown for other garnets. PM, calculated Lu and Yb abundances for garnet in a model peridotite (12 wt.% gar, 13 wt.% cpx, 17 wt.% opx) with primitive whole-rock REE abundances (Hofmann, 1988; Sun and McDonough, 1989) assuming $Lu^{gar/cpx} = 25$, $Yb^{gar/cpx} = 20$, $Lu^{cpx/opx} = 6$. The modal abundances and intermineral REE ratios for PM are close to average values for most fertile Vitim xenoliths and may not be appropriate for peridotites equilibrated at different P-T conditions. Data sources: Vitim, Table 2, Ionov (2004), Ionov et al. (2005); Mongolia, electronic annex; China, Xu et al. (2000; 2003); Pali-Aike, Kempton et al. (1999); Stern et al. (1999).

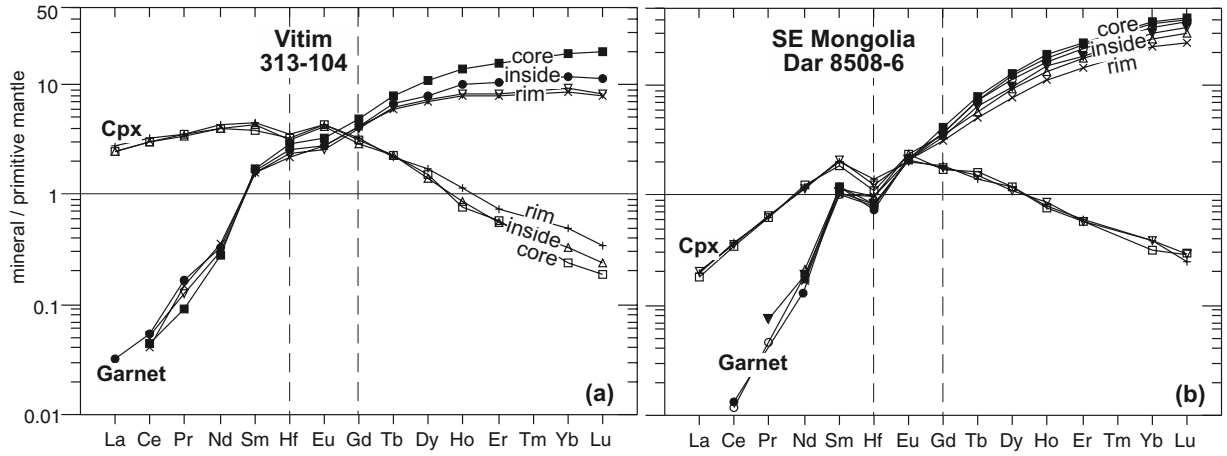

Fig. 5. Primitive mantle-normalized (Hofmann, 1988) REE and Hf abundances in core-rim profiles across garnet and clinopyroxene grains in two peridotite xenoliths determined by LA-ICPMS (electronic annex).

samples 313-54 and 313-102 (Table 3) confirm the strong Lu and Y zoning in garnet 313-102, and the lack of zoning in garnet 313-54 for REE, Ti, Sr, Y and Nb. The new analyses also yield slightly lower Lu and Y abundances in clinopyroxene cores than in the rims, but show no zoning for other elements.

Both SIMS profiles and laser ablation analyses in grain mounts are available for garnet in sample 313-54. The two SIMS profiles yield similar average Lu values of ~0.35 ppm (Ionov, 2004) and ~0.40 ppm (Table 3) in each grain whereas the Lu values in LA-ICPMS analyses of two other grains are distinct (0.41 and 0.54 ppm, Table 2). Because both SIMS profiles show no zoning, the difference between the two LA-ICPMS analyses is likely to be due to grain-to-grain HREE variations. Garnet analyses in some other xenoliths (313-6, Table 2) found no significant grain-to-grain differences in HREE. Heterogeneous garnets appear to be less common in garnet lherzolites than in garnet-spinel xenoliths (garnet is heterogeneously distributed in the latter as well, Fig. 2 b-d).

Figure 5 shows REE+Hf patterns in profiles across garnet and clinopyroxene grains in another Vitim xenolith (313-104) and in a lherzolite from SE Mongolia obtained by LA-ICPMS (electronic annex). Garnets in both xenoliths have continuous core-rim zoning for REE heavier than Gd, with Lu abundances 1.7–2.6 times higher in the core than near rims. Clinopyroxene 313-104 has a small-scale HREE zoning, which mirrors that in the garnet (Fig. 5a), like for xenolith 313-102 (Table 3). The 'mirror' HREE zoning in the clinopyroxene and garnet seems to be inconsistent with equilibrium cpx/gar distribution assuming constant partition coefficients. One should note however that clinopyroxene in both xenoliths has major element zoning indicating recent heating while garnet rims are replaced by HREE-poor kelyphite apparently as a result of the heating

Table 3. SIMS analyses of minerals (grain profiles in thin sections) in two Vitim garnet lherzolites.

	313-54 garnet			313-54, clinopyroxene			313-102, garnet			313-102, clinopyroxene		
	Core av.2	Int	Rim av.2	Core av.2	Int	Rim av.2	Core av.2	Int	Rim av.2	Core av.2	Int	Rim av.2
Ti	1302	1283	1265	2074	2040	2024	1010	973	1015	2800	2774	2682
Sr	0.13	0.15	0.13				0.20	0.25	0.20	62.1	62.8	60.4
Y	30.5	29.5	29.8	3.47	4.16	4.28	35.7	28.1	25.2	3.66	3.77	4.73
Zr				20.7	20.8	20.3						
Nb	0.07	0.06	0.06							0.81	0.86	
Ba	0.00	0.04	0.03	0.03	0.87	0.50				0.05	0.24	
La				1.44	1.95	1.73	0.013	0.008	0.013	0.89	0.88	0.90
Ce				4.30	5.19	4.83						
Nd	0.46	0.50	0.49	4.30	4.49	4.49	0.32	0.29	0.30	3.45	3.44	3.54
Sm	0.65	0.54	0.57	1.46	1.55	1.53				1.34	1.29	
Eu	0.38	0.37	0.38	0.54	0.55	0.55				0.45	0.46	
Gd	2.20	2.05	2.03	1.56	1.69	1.66				1.17	1.16	
Tb	0.53	0.52	0.52	0.21	0.22	0.22	0.47	0.46	0.42	0.19	0.19	0.21
Dy	4.17	4.15	4.19	0.93	1.07	1.08				0.79	0.76	
Er	3.03	2.96	2.97	0.29	0.35	0.37				0.25	0.24	
Yb	2.66	2.80	2.91	0.12	0.20	0.21				0.11	0.11	
Lu	0.40	0.40	0.42	0.012	0.015	0.016	0.91	0.50	0.45	0.019	0.024	0.035
Hf	0.43		0.42	0.93	0.86	0.86	0.44		0.61	0.79		0.82

Int, intermediate between the rim and the core.

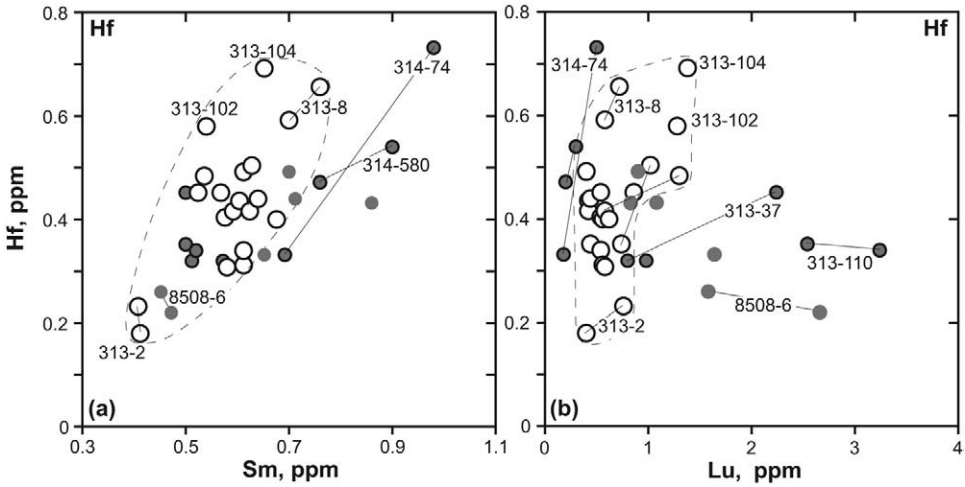

Fig. 6. Plots of Hf vs. Sm (a) and Lu (b) in garnet from xenoliths: large empty circles, Vitim garnet lherzolites; small grey-filled black circles, Vitim garnet-spinel lherzolites; small grey circles, lherzolites from Mongolia. Straight lines connect individual analyses in xenoliths with heterogeneous garnets; dashed lines contour Vitim garnet lherzolites. Data sources same as in Figure 4.

(Ionov, 2004). Thus, breakdown of garnet rims releases HREE that are then taken up by outer parts of clinopyroxene grains. An ongoing SIMS study has documented HREE zoning in garnets from other Vitim xenoliths (Mocek et al., 2004). In summary, our results show that HREE-zoned garnets are common in the central Asian xenoliths; they may be widespread in off-craton garnet lherzolites worldwide.

Hf abundances in garnet in the majority of the Vitim and Mongolian xenoliths range from 0.3 to 0.5 ppm, a few samples show a broader range (0.2–0.75 ppm). Garnets with >0.5 ppm Hf are from the three most fertile Vitim lherzolites (4.4–4.8% Al_2O_3; Ionov et al., 2005) while garnets with <0.3 ppm Hf are from the two most refractory samples (Fig. 6a). Hence, positive correlation of Hf with Sm (Fig. 6a) is consistent with moderately incompatible behavior of both elements during partial melting of fertile mantle. The very broad Hf range in garnet from sample 314-74, and possibly some scatter on the Hf-Sm plot, are most likely due to local modal variations (Fig. 2) causing re-distribution of Hf and Sm between garnet and pyroxenes. Unlike for the Hf-Sm pair, Hf abundances in garnet show no general correlation with Lu (Fig. 6b). Hf abundances tend to be higher in Lu-rich grains in some xenoliths with heterogeneous garnets, but they show no variation (sample 313-105; Table 2) or the opposite Hf-Lu relationships in other samples (Fig. 6b). In some xenoliths, garnets have a range of Lu/Hf values. Because of the small number of grains analyzed in each sample, these data may not cover the whole range of HREE variation in individual xenoliths. For example, comparisons of measured and calculated whole-rock HREE indicate that garnets with much lower Lu abundances than those given in Table 2 may be common in xenolith 313-110.

Overall, the Lu and Hf variations in garnet in the majority of >20 central Asian xenoliths analyzed in this and related studies (Ionov, 2004; Ionov et al., 2005) are much broader than the analytical uncertainty (r.s.d. ≤3% at ≥0.3 ppm, Table 2). Furthermore, Lu levels in some xenoliths are higher than those estimated for garnet in normal fertile peridotite mantle.

5.2. Hf Isotope Compositions

Hf isotope compositions were determined in minerals of ten Vitim xenoliths: four garnet, three garnet-spinel and three spinel peridotites. Both garnet and clinopyroxene were analyzed for three garnet and one garnet-spinel lherzolite. Separation of sufficient amounts of pure garnet from garnet-spinel peridotites 314-74 and 314-580 was not possible because of small grain size, low modal abundances and high degrees of alteration (kelyphite) of garnet. Acid-leached, kelyphite-rich garnet fraction 314-580 obtained by magnetic separation was analyzed to assess the Hf isotope composition of garnet breakdown products.

The Lu-Hf isotope data are given in Table 4 together with average Lu and Hf values for clinopyroxene and garnet from LA-ICPMS analyses (Table 2), as well as solution ICPMS and INAA data on Lu and Hf in pure mineral separates available for several xenoliths from earlier work (Ionov et al., 1993; Ionov et al., 2005). The Lu and Hf abundances determined by isotope dilution (ID) agree well with those from the other three methods in nearly all cases except for Lu in garnet 313-54 and in clinopyroxene 314-56. The distinct ID values for these two samples may reflect either sample heterogeneity or analytical problems because Lu abundances from the other three methods agree well (0.48–0.51 ppm for garnet 313-54 and 0.34–0.37 ppm for cpx 314-56; Table 4). Apart from these rare discrepancies, the generally good match between the laser and solution ICPMS analyses on the one hand and the ID (as well as INAA) data on the other hand indicates that the ICPMS analyses may provide satisfactory Lu/Hf estimates for Lu-Hf isotope studies in cases when ID data are not available.

As illustrated in Figure 7, both $^{176}Lu/^{177}Hf$ and $^{176}Hf/^{177}Hf$ are significantly higher in garnet than in coexisting clinopyroxene. Bi-mineral isochron Lu-Hf ages for four xenoliths (Table 4) range from 24 to 84 Ma. These estimates should be considered with caution because Lu-Hf zoning and intergrain variations may affect their accuracy. Nevertheless, all of them are

Table 4. Hf-isotope ratios, Lu and Hf abundances and age estimates for Vitim xenoliths.

	Hf,ppm				Lu,ppm						$^{176}Hf^{177}Hf$	2σ	Gar-Cpx ages, Ga		WR model ages, Ga	
Sample No.	ID	LA	Sol.ICP	INAA	ID	LA	Sol.ICP	INAA	$^{176}Lu/^{177}Hf$ ID	$^{176}Lu/^{177}Hf$ LA	mineral	error	ID	LA	ID	LA/sol
Garnet peridotites:																
313-6 Cpx	1.05	1.10		1.02	0.018	0.018		0.048	0.002	0.002	0.283304	0.000010	0.077	0.084	23	–
313-6 Gar	0.48	0.49		0.41	0.42	0.39		0.46	0.124	0.113	0.283483	0.000010				
313-54 Cpx	0.97	0.93	1.00	0.87	0.021	0.017	0.021	0.034	0.003	0.003	0.283429	0.000009	0.046	0.057	1.2	1.2/2.6
313-54 Gar	0.45	0.43	0.39	—	0.69	0.48	0.49	0.51	0.217	0.158	0.283620	0.000015	0.035			
313-54 Gar2	0.44				0.73				0.235		0.283586	0.000011				
313-102 Gar	0.61	0.58			1.38	1.28			0.323	0.313	0.284008	0.000011				
313-102 Gar2	0.56				1.15				0.291		0.283947	0.000015				
313-105 Cpx	0.96	1.01	0.99	1.05	0.023	0.027	0.025	0.015	0.003	0.004	0.283324	0.000010	0.031	0.036	1.34	2.3/4
313-105 Gar	0.49	0.46	0.48	0.50	0.70	0.58	0.60	0.64	0.204	0.179	0.283445	0.000016				
Garnet-spinel peridotites:																
313-110 Cpx*		0.89				0.013				0.002	0.283555	0.000010		0.024		0.21
313-110 Gar*		0.35				2.85				1.156	0.284094	0.000017				
314-74 Cpx*		0.50		0.52		0.079		0.088		0.022	0.284031	0.000017				
314-580 Cpx*		1.25		1.23		0.017		0.059		0.002	0.283307	0.000010				
314-580 Gar*		0.44		—		0.25		0.40		0.081	/0.283286/	0.000012				
Spinel peridotites:																
314-56 Cpx	1.25	1.24	1.26	1.24	0.29	0.37	0.35	0.34	0.033	0.042	0.283306	0.000008			868	3.0/1.7
314-58 Cpx*		1.11		1.33		0.35		0.38		0.044	0.283341	0.000006				2.7
314-59 Cpx*		0.83	0.89	0.92		0.23	0.23	0.22		0.039	0.283396	0.000014				5.9

Gar2 are duplicate garnet separates which contain small amounts of kelyphite. Gar 314-580 contains >10% kelyphite.
LA-ICPMS data are from Table 2 except for 313-102 (Ionov, 2004). Solution ICPMS data are from Ionov et al. (2005). INAA data are from Ionov et al. (1993).
* Hf-isotope analyses done at Brussels (Lu and Hf abundances were not determined). ID, isotope dilution; LA, laser ablation ICPMS; Sol.ICP, solution ICPMS.

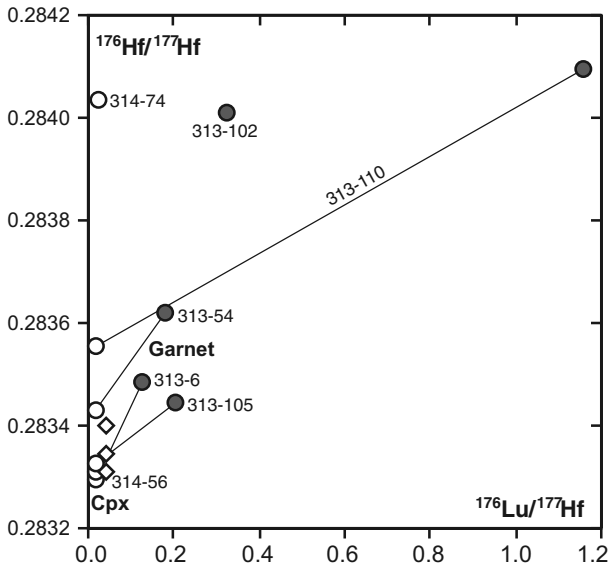

Fig. 7. Plot of $^{176}Lu/^{177}Hf$ vs. $^{176}Hf/^{177}Hf$ for clinopyroxene (empty circles, cpx from garnet-bearing rocks; rhombs, cpx from spinel peridotites) and garnet (filled circles) in Vitim xenoliths. Coexisting minerals are connected with solid lines.

higher than the eruption age of the host volcanic rock (16 Ma). It follows that garnet and clinopyroxene were not in complete equilibrium with respect to the Lu-Hf isotope system when the xenoliths were brought up to the surface, even in rocks with homogeneous Lu and Hf distribution in minerals, like 313-6 (Table 2). This may be due to inability to attain intermineral isotopic equilibrium in the coarse-grained mantle rocks by diffusion at relatively low (~1000°C) ambient temperatures (Van Orman et al., 2002a; Bedini et al., 2004). The kelyphite-rich garnet fraction of xenolith 314-580 yielded lower $^{176}Hf/^{177}Hf$ than for clinopyroxene from the same sample. This result appears to indicate that the Hf isotope composition of kelyphite is distinct from that of its garnet predecessor because the latter has higher $^{176}Lu/^{177}Hf$ and therefore may not have lower $^{176}Hf/^{177}Hf$ than coexisting clinopyroxene.

Hf isotope compositions of whole-rock Vitim xenoliths are shown in Figure 8 plotted against $^{143}Nd/^{144}Nd$ and $^{87}Sr/^{86}Sr$. On the Hf-Nd isotope diagram (Fig. 8a), the majority of the Vitim samples plot at or near the most radiogenic end of the midocean-ridge basalt (MORB) field and way beyond towards higher $^{143}Nd/^{144}Nd$ and/or $^{176}Hf/^{177}Hf$. Garnets from samples 313-102 (reproduced in duplicate) and 313-110 have particularly high $^{176}Hf/^{177}Hf$; nevertheless, the whole-rock estimate for 313-110 is much lower than the garnet value because Hf resides mainly in clinopyroxene (Table 2), which has lower $^{176}Hf/^{177}Hf$. Clinopyroxene 314-74 has very radiogenic Hf; $^{176}Hf/^{177}Hf$ in coexisting garnet (not measured), and therefore in the whole-rock sample, must be even higher because of higher Lu/Hf (Table 2). Therefore, sample 314-74 has the strongest deviation among the Vitim xenoliths above the mantle Hf-Nd array (which is based on oceanic basalt data; Hofmann, 2003). This is similar to the Hf-Nd isotope decoupling shown by some other cratonic and off-craton peridotites (Schmidberger et al., 2002; Pearson et al., 2003; Bedini et al., 2004; Bizimis et al., 2004). Clinopyroxene 314-580 plots within the MORB field on the Hf-Nd isotope diagram despite fairly high LREE (Fig. 3b), which may indicate a contribution from metasomatism. The whole-rock $^{176}Hf/^{177}Hf$ for that sample must be higher if garnet contribution is taken into account (garnet composition is not available). All Vitim peridotites we measured plot far from the field of Vitim Cenozoic basalts reported by Johnson et al. (2005).

Between the two plots shown in Figure 8, it is evident that overall, the majority of the Vitim xenoliths have fairly radiogenic Hf and Nd isotope compositions and low $^{87}Sr/^{86}Sr$. A small number of Vitim xenoliths are akin to MORB, but the majority of them extend beyond the most depleted extremity of

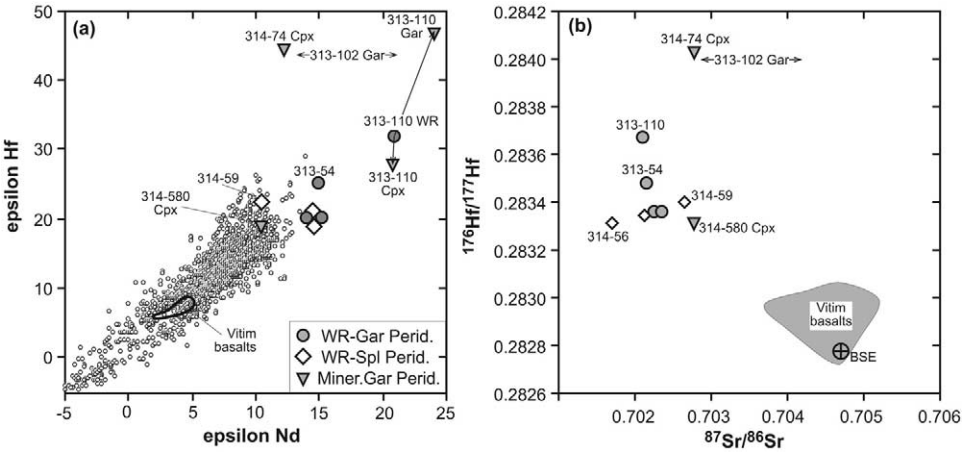

Fig. 8. Plot of $^{143}Nd/^{144}Nd$ (a) and $^{87}Sr/^{86}Sr$ (b) vs. $^{176}Hf/^{177}Hf$ for Vitim xenoliths. Whole-rock (WR) values for spinel peridotites are assumed to be the same as in their clinopyroxene; whole-rock values for garnet peridotites were calculated from garnet and clinopyroxene analyses and modal abundances. Data for minerals only are shown for three garnet-bearing xenoliths, for which analyses of either garnet or clinopyroxene are available. $^{143}Nd/^{144}Nd$ and $^{87}Sr/^{86}Sr$ values are from Ionov et al. (2005); they are not available for garnet 313-102. Also shown is a compilation of published MORB and OIB data (small empty circles; J. Blichert-Toft) and a field of Vitim basalts from Johnson et al. (2005).

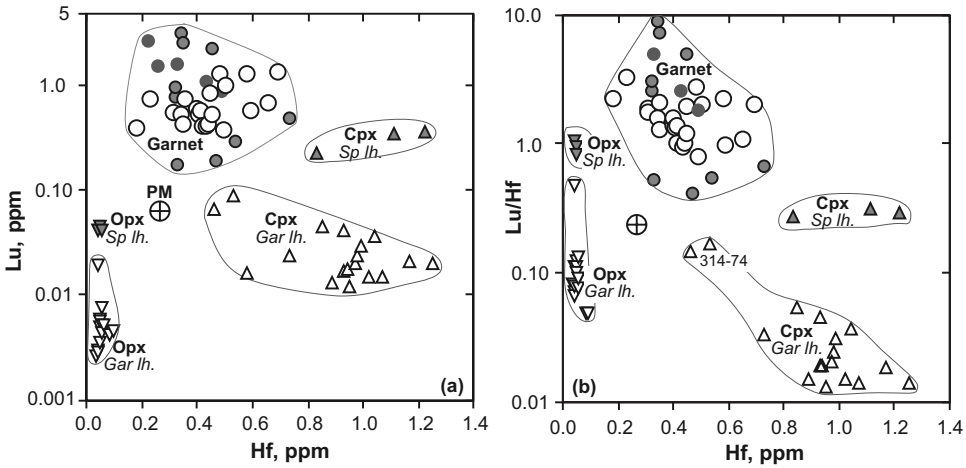

Fig. 9. Plots of Hf vs. Lu (a) and Lu/Hf (b) in minerals. Data sources and symbols for garnet same as in Figure 4. Triangles are pyroxenes from Vitim xenoliths (grey-filled for spinel lherzolites).

the MORB field. In this respect, they resemble xenoliths from some other cratonic and off-craton peridotite suites (Schmidberger et al., 2002; Bizimis et al., 2004), but the main difference is that Vitim xenoliths, which have high $^{176}Hf/^{177}Hf$, also tend to have higher $^{143}Nd/^{144}Nd$ (Ionov and Weis, 2002; Pearson et al., 2003) because they have not been significantly affected by metasomatic enrichments in LREE.

6. DISCUSSION

6.1. Intermineral Partitioning of Hf and Lu in Spinel and Garnet Peridotites

The residence of Hf and Lu in peridotites provides important information for Hf isotope studies, in particular, because whole-rock Hf isotope compositions of mantle peridotites are usually estimated from mineral data. Hf abundances in whole-rock peridotites are quite low (≤0.2 ppm), rendering it difficult to separate enough Hf (usually ~50 ng) for reliable isotope analyses (Blichert-Toft, 2001; Münker et al., 2001). Furthermore, whole-rock xenolith samples may be contaminated either by infiltration of host magmas or by posteruption alteration, potentially affecting both Lu/Hf and $^{176}Hf/^{177}Hf$. Hf and Lu residence in the Vitim xenoliths analyzed for Hf isotopes can be quantitatively assessed using LA-ICPMS analyses (available for all major minerals) and supplemented by whole-rock solution ICPMS data from earlier work (Ionov, 2004; Ionov et al., 2005). Importantly, no Hf-rich accessory minerals of mantle origin have been found in the Vitim peridotite xenoliths in this or earlier studies.

Clinopyroxene contains more Hf than other minerals of garnet and spinel lherzolites (Fig. 9). Average Hf abundances are 2–2.5 times higher in clinopyroxene than in coexisting garnet from central Asian garnet lherzolite xenoliths (Table 2; electronic annex). In addition, the modes of clinopyroxene in the garnet lherzolites are equal to or higher than those of garnet (Table 1). As a result, clinopyroxene is by far the most important host of Hf in fertile garnet lherzolites from Vitim (and probably elsewhere), making up 70–75 wt.% of their whole-rock Hf budget (Table 2). The share of Hf hosted by orthopyroxene in fertile garnet lherzolites ranges from 4 to 6 wt.% and is somewhat higher in garnet-spinel rocks with low modal clinopyroxene and garnet, like 314-74. The Lu/Hf values are much higher in garnet (0.6–8.1) than in coexisting clinopyroxene (0.01–0.03) and orthopyroxene (0.06–0.11) (Fig. 9b). In general, the orthopyroxene contribution to whole-rock $^{176}Hf/^{177}Hf$ and Lu/Hf in fertile garnet lherzolites is of the same order of magnitude as uncertainties involved in estimating modal abundances of garnet and clinopyroxene and can probably be neglected.

Orthopyroxene hosts 7–9 wt.% of Hf in fertile spinel lherzolites from Vitim (Table 2). This is higher than in garnet lherzolites mainly because of lower modal opx/cpx in the latter. Even more Hf resides in orthopyroxene in refractory peridotites, which have higher modal opx/cpx because clinopyroxene is consumed faster during melt extraction (Walter, 2003). For example, ≥20 wt.% of total Hf would reside in orthopyroxene in a cpx-poor lherzolite with ≤5 wt.% clinopyroxene and ~25 wt.% orthopyroxene. The share of Lu hosted by orthopyroxene in spinel lherzolites (~20% in fertile Vitim xenoliths) is higher than that of Hf. The opx/cpx abundance ratios for Lu (0.12–0.25) in spinel lherzolites from Vitim are much higher than for Hf (0.04–0.06). As a result, Lu/Hf values in orthopyroxene (0.8–1.0) are 3–4 times higher than in coexisting clinopyroxene (0.27–0.31) (Fig. 9b). Overall, the contribution of orthopyroxene to the whole-rock Lu/Hf and Hf inventory of spinel peridotites is significant and has to be taken into account, in particular for refractory peridotites and those with old emplacement ages. Whole-rock $^{176}Hf/^{177}Hf$ for fertile xenoliths in young volcanic rocks (such as many samples from this study) can probably be well constrained from clinopyroxene analyses alone.

Hf abundances in olivine are very low (≤3 ppb; Table 2, electronic annex). Despite high modal abundances, olivine is negligible in the whole-rock budget of Hf in normal peridotites (e.g., ~0.2 wt.% for 314-56; Table 2). Speculations that hypothetical interstitial apatite may be a significant host for Hf in garnet peridotites (Bedini et al., 2004) are inconsistent with low

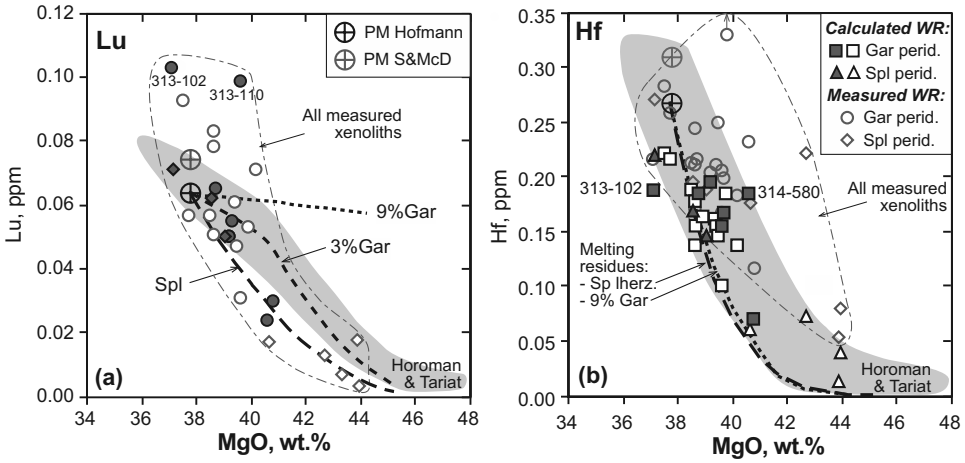

Fig. 10. Co-variation diagrams for Lu (a) and Hf (b) vs. MgO for whole-rock Vitim peridotite xenoliths. Circles and rhombs are whole-rock analyses of Lu and Hf. Squares and triangles in (b) show Hf abundances calculated from mineral analyses and modal data for garnet and spinel xenoliths respectively; filled symbols are samples analyzed for Hf isotopes. Thin dashed line contours the field of measured whole-rock compositions (Ionov, 2004; Ionov et al., 2005). Thick dashed lines are model residues after fractional partial melting (1–23%) of primitive mantle in spinel and garnet facies (modal garnet before melting is shown) calculated using an algorithm and partition coefficients from Takazawa et al. (2000). Black and gray circles with a cross are primitive mantle compositions after Hofmann (1988) and Sun and McDonough (1989) respectively.

Hf in apatite from peridotite xenoliths (Ionov et al., 1997; Bedini et al., 1999).

6.2. The Behavior of Lu and Hf During Partial Melting

Another important issue for the interpretation of Lu-Hf isotope data on peridotites is whether the abundances of the parent-daughter elements are controlled by partial melting or, alternatively, by metasomatism, melt percolation or yet other processes after the formation of melting residues. Petrographic and major element data indicate that the Vitim peridotites were originally formed as residues after very low to moderate degrees of melt extraction from a fertile protolith (Ionov et al., 1993; Ionov, 2004) and have not been significantly affected by metasomatism. The LREE-depleted patterns of minerals in the majority of the xenoliths appear to preserve the partial melting record as well (Fig. 3). Only one sample in this study may record apparent trace element effects of metasomatism (314-580; Fig. 3b).

Whole-rock abundances of Lu and Hf are shown in Figure 10 vs. MgO as a partial melting index. Lu values measured by solution ICPMS (Ionov, 2004; Ionov et al., 2005) in the majority of Vitim xenoliths plot close to model primitive mantle compositions and to calculated melting residue trends in spinel and garnet-spinel fields (Fig. 10a). By contrast, whole-rock Lu abundances in xenoliths with HREE-rich garnets (including 313-102 and 313-110; Figs. 3c-d and 4a) are higher than in other fertile xenoliths and cannot be derived by partial melting of primitive mantle (Ionov, 2004). The measured whole-rock Lu values are similar to those calculated from modal data and mineral analyses (Table 2) for nearly all Vitim xenoliths except 313-110 (calculated Lu_{WR} ~0.26 ppm is too high). It is possible that LA-ICPMS analyses of garnet in this modally heterogeneous sample (Fig. 2c-d) are not representative of the whole range of garnet compositions (i.e., only HREE-rich grains were analyzed).

In contrast to Lu, measured whole-rock Hf abundances are systematically higher than those calculated (Table 2). The difference is small for some xenoliths (e.g., 313-6) but is significant (10–30%) for the majority of xenoliths in this study and is nearly two-fold for sample 314-74. The enrichments for Hf and less compatible elements are most likely related to veining and alteration of the xenoliths during and after their transport to the surface (Ionov, 2004). In particular, dark secondary material is apparent inside olivine and along grain boundaries in Figure 2. In any case, the calculated whole-rock Hf and Lu/Hf values obviously provide much better estimates for the Vitim peridotites before their transport from the mantle than the measured values. Here, we re-assess some modeling results of Ionov (2004) with regard to Hf abundances and Lu/Hf by using the calculated whole-rock values instead of whole-rock analyses. The estimated "preeruption" whole-rock Hf values provide a substantially better fit to melting trends (Fig. 10b) than the typically higher measured Hf abundances shown in Figures 11c and 12b of Ionov (2004). Only the calculated whole-rock Hf for xenolith 314-580 plots well above the melting trend, possibly due to a metasomatic enrichment.

In summary, new mineral data and modeling from this study further indicate that high whole-rock Lu abundances in some garnet-bearing Vitim peridotites are inconsistent with partial melting origins. Furthermore, the high whole-rock HREE are matched with HREE-enrichments in garnets and are not related to unusual modal compositions (e.g., modal garnet in 313-110 is not higher than in other Vitim xenoliths). Conversely, the anomalously high and fractionated HREE in garnets from those rocks cannot be produced by intermineral partitioning (HREE reside mainly in garnet anyway because gar/cpx ratios for HREE are very high) and reflect strong whole-rock HREE

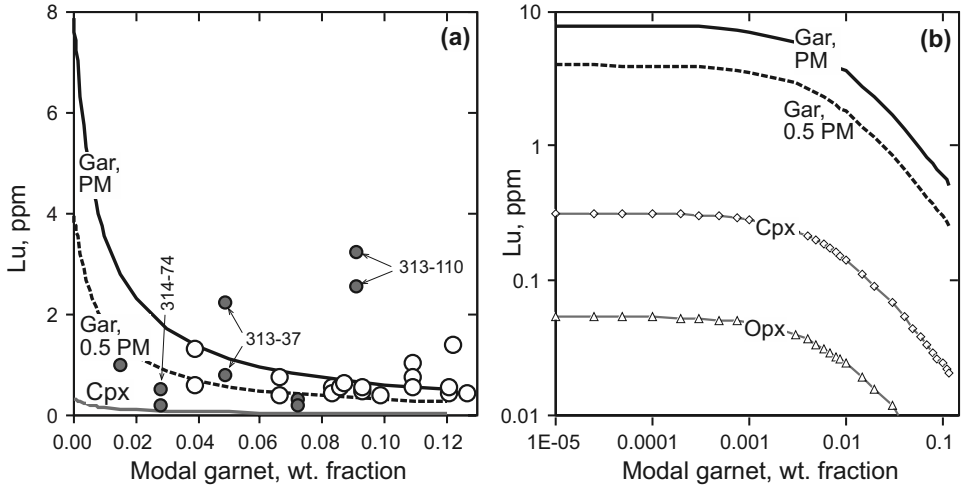

Fig. 11. (a) Calculated Lu abundances in garnet during spinel-garnet phase transition in a model primitive mantle (PM) lherzolite (Lu_{WR} = 0.0637 ppm) as a function of modal garnet. Initial spinel lherzolite contains 16 wt.% cpx and 25 wt.% opx. Garnet-forming reaction is: 0.29 spl + 0.74 opx + 0.22 cpx = 1 gar + 0.26 ol (Ionov et al., 1993) to produce a garnet lherzolite with 12 wt.% gar, 13 wt.% cpx, 17 wt.% opx (a typical mode for fertile Vitim garnet lherzolites). $Lu^{gar/cpx}$ = 25, $Lu^{cpx/opx}$ = 6. Dashed line shows Lu in garnet for a peridotite with 0.5 PM Lu abundance (0.032 ppm). (b) Same as (a) on a logarithmic scale. Also shown are data for Vitim xenoliths (with highest and lowest Lu values in garnet from each sample if they differ by >20%); data sources and symbols same as in Figure 6.

enrichments in those samples, which set them aside from the rest of the xenoliths. There is no chemical, petrographic or isotope evidence that metasomatism or late-stage disequilibrium melting play a role in the HREE enrichments.

6.3. Constraints on Lithospheric Ages from Hf-Isotope Data

Lu-Hf garnet-clinopyroxene age estimates for three garnet lherzolite xenoliths from Vitim (31-84 Ma; Table 4) are higher than corresponding bi-mineral Sm-Nd ages (24-42 Ma; Ionov and Jagoutz, 1988; Ionov et al., 2005); both ranges are somewhat higher than the likely eruption age of the host volcanic rock from K-Ar dating (15-18 Ma). A fairly low Lu-Hf age estimate (24 Ma) obtained for garnet-spinel xenolith 313-110 is most likely incorrect because average Lu, and thus Lu/Hf, values for the garnet in this sample obtained by LA-ICPMS appear to be too high. The use of a Lu value for the garnet (~1.2 ppm) consistent with the measured whole-rock Lu abundance (Table 2) yields a garnet-clinopyroxene Lu-Hf age of ~60 Ma. The systematically high (compared to the eruption age) Lu-Hf (as well as Sm-Nd) bi-mineral ages obtained for the four Vitim xenoliths appear to indicate that Hf (and Nd) isotope compositions of clinopyroxene and garnet were not in complete equilibrium when the xenoliths were entrained in their host magma. Likely reasons for this could be the large size and irregular distribution of garnet in the peridotites (Fig. 2). Hf diffusion rates are poorly known. Recent experimental data on REE diffusion rates indicate closure temperatures for Nd in diopside (crystals 1 mm in diameter cooling at 1 to 100°C million $years^{-1}$) of 960–1120° (Van Orman et al., 2002a); the lower half of this range overlaps the T range for the Vitim xenoliths (Table 1). The higher Lu-Hf than Sm-Nd garnet-clinopyroxene age estimates were also noted in other mantle xenolith suites (e.g., Bedini et al., 2004) and may indicate slower diffusion rates and/or higher closure temperatures for Hf than for Nd.

The Hf-Nd-Sr isotopic signatures of the Vitim peridotites are distinct from those of their host basalts. For the majority of the xenoliths they are also distinct from the modern source regions of oceanic basalts (Fig. 8) and cannot have been generated recently from the convecting asthenospheric mantle. Therefore, the Lu-Hf isotope data are generally consistent with the antiquity of the sub-Vitim lithospheric mantle, which may have been produced by an ancient partial melting event as suggested earlier from Sr-Nd and Os isotope data (Ionov and Jagoutz, 1988; Pearson et al., 2004).

The age of that event may, in principle, be constrained from the Lu-Hf isotope system. Unfortunately, the whole-rock Lu-Hf isotope data for three xenoliths with the highest $^{176}Hf/^{177}Hf$ in their minerals are either missing or imprecise and thus unsuitable for defining an isochron age. The lack of data on clinopyroxene 313-102 and garnet 314-74 makes it impossible to calculate whole-rock $^{176}Hf/^{177}Hf$ for these two xenoliths. Garnet and whole-rock Lu/Hf in sample 313-110 are poorly constrained. Most importantly, high Lu in xenoliths 313-102 and 313-110 cannot be produced by partial melting of fertile mantle (section 6.2), therefore Lu-Hf isotope systematics in these two samples may have been affected by other events.

The $^{176}Hf/^{177}Hf$ range in the remainder of the xenoliths is too narrow (0.2833–0.2835) to define a good isochron. Nevertheless, their depletion ages can be estimated using the model age approach relative to primitive mantle ($^{176}Hf/^{177}Hf$, 0.282772; $^{176}Lu/^{177}Hf$, 0.0332) (Blichert-Toft and Albarède, 1997). The model ages for garnet lherzolites 313-54 and 313-105 range from 1.2 to 4 Ga depending on which Lu/Hf values are used (ID, LA- or solution ICPMS, Table 4). Model age estimates for spinel lherzolites involve additional uncertainties

because a larger proportion of Hf resides in orthopyroxene (not analyzed for Hf isotopes) and because orthopyroxene affects whole-rock Lu/Hf more than for garnet peridotites (section 6.1). For example, an age of 3 Ga is obtained for sample 314-56 based on clinopyroxene data only, but a much lower value (1.7 Ga) is obtained using a whole-rock Lu/Hf calculated taking into account Lu and Hf in orthopyroxene. The latter estimate however is a minimum age because orthopyroxene must have more radiogenic $^{176}Hf/^{177}Hf$ than clinopyroxene based on its higher Lu/Hf. Overall, robust Lu-Hf depletion ages cannot be obtained for the Vitim xenoliths, mainly because of problems with assessing their bulk Lu/Hf and $^{176}Hf/^{177}Hf$ related to heterogeneous mineral compositions and the lack of data for orthopyroxene. It is important, however, that all relevant estimates yield ancient, mainly Proterozoic ages (Table 4). Therefore, a general link with the Precambrian continental lithosphere seems reasonable from the Lu-Hf data, as well as from Sr-Nd and Re-Os data (Ionov and Jagoutz, 1988; Pearson et al., 2004). A large number of studies have reported old formation ages for igneous and metamorphic crustal rocks in the vicinity of the Vitim plateau, ranging from Paleoproterozoic to late Archean (see Kovalenko et al., 1991 and Ionov et al., 2005 for reviews).

One can speculate that the HREE-rich xenoliths initially experienced the same melting episode as the remainder of the Vitim peridotites and were later enriched in Lu by some other process. Constraining the age of the latter hypothetical event is complicated because the time-integrated signature of Lu-Hf isotope evolution following such an event must be superimposed on the signature of earlier Lu-Hf evolution (at lower Lu/Hf) after the initial partial melting. The model ages obtained for xenolith 313-110 are quite young (0.2–0.5 Ga depending on the choice of whole-rock Lu/Hf); they represent maximum age estimates for the Lu enrichment because the calculation ignores the effects of earlier melting events. These ages are qualitatively consistent with a mid to late Phanerozoic Lu enrichment, i.e., during or after the abundant granitic magmatism in the Vitim region (section 2).

6.4. Possible Origins for Anomalous HREE Distribution in Mantle Peridotites

New trace element data in this study indicate that anomalously high HREE abundances and HREE/MREE are common in garnets and whole-rock peridotites in the off-craton lithospheric mantle beneath central Asia (and possibly elsewhere). This intriguing chemical feature must have important effects on the Lu-Hf isotope system. Previous models for creating chemical and isotope heterogeneities in mantle peridotites, which cannot be explained by partial melting or metasomatism, usually invoked mixing of variously depleted peridotite protoliths with other rock types, like pyroxenites and eclogites (e.g., Becker, 1996; Pearson and Nowell, 2004). Whilst the mixing model is appealing and basically plausible, it requires a series of poorly constrained assumptions: (1) availability of required rock types; (2) effective mixing and annealing of those rocks in the lithospheric mantle; (3) specific chemical and isotopic compositions, etc. Some of these assumptions are hard to reconcile with petrographic, chemical and isotope data on the central Asian xenoliths.

Mechanical mixing of peridotites with pyroxenites or other rocks requires strong and long-lived shear forces that do not exist in the lithospheric mantle beyond major faults or plate boundaries. There is no textural evidence for deformation to support such mixing in the mantle beneath Vitim (Fig. 2; Kern et al., 1996). Importantly, widespread mixing would also eliminate chemical and isotope variations produced by the ancient partial melting (Ionov et al., 1993; 2005). It follows that the mixing could only have taken place before the 2 Ga melting event, which appears to have created the mantle lithosphere beneath Vitim (Ionov and Jagoutz, 1988; Pearson et al., 2004). That large-scale melting event, however, is likely to have strongly overprinted and re-equilibrated preexisting chemical heterogeneities. Finally, Lu-Hf data on xenolith 313-110 indicate that the Lu enrichment cannot be older than 0.2–0.5 Ga.

Ionov (2004) explored a model of metamorphic garnet segregation in the Vitim peridotite mantle. He argued that addition or removal of small amounts (<5%) of garnet with 0.5–0.6 ppm Lu to/from fertile or moderately depleted peridotites cannot account for anomalously low or high Lu in some Vitim xenoliths, while higher garnet addition rates would yield too high Al_2O_3 in the rocks. The results of the modeling are also valid for mixing of peridotites with Al-rich pyroxenites if the latter do not have much higher Lu/Al. Furthermore, the mixing models cannot explain the origin of those (mainly spinel-facies) peridotites from Vitim that have anomalously low HREE and HREE/MREE in whole-rocks and clinopyroxenes; such rocks appear to be complementary to the HREE-enriched garnet peridotites (Ionov, 2004).

To produce hybrid HREE-enriched peridotites, the hypothetical pyroxenites must have both high HREE and high HREE/MREE (as well as high Lu/Al). Similar compositions were reported for pyroxenites from some peridotite massifs (Becker, 1996; Pearson and Nowell, 2004); they may represent partial melting residues of subducted oceanic crust. On the other hand, such chemical features are not common among normal mantle-derived magmatic liquids or pyroxenite veins of magmatic origin in the lithospheric mantle. In particular, such rocks have not been reported in studies of composite and pyroxenite xenoliths in the Vitim volcanic field (Litasov et al., 2000; Ashchepkov and André, 2002). Sr-Nd-Os isotope data on the peridotite xenoliths (Pearson et al., 2004; Ionov et al., 2005) yield no evidence for mixing with pyroxenites, and there is no obvious evidence for subduction in the Vitim mantle.

The strongest argument to assign the anomalously high HREE in mantle peridotites to mixing with pyroxenites appears to be the apparent absence of any other mantle events that can produce large increases in HREE and HREE/MREE. Here we argue, following Ionov (2004), that the latter assumption may be invalid.

6.5. HREE Fractionation During Spinel-Garnet Phase Transition in the Mantle

HREE abundances in garnet are mainly controlled by two parameters: whole-rock HREE and modal garnet. At a given whole-rock Lu, the Lu abundance in garnet should be inversely correlated with modal garnet because garnet is by far the most important Lu host. We calculate Lu abundances in minerals of fertile lherzolites during spinel-garnet phase transition as a function of modal garnet using average gar/cpx/opx ratios for

Lu ($Lu^{gar/cpx}$ = 25, $Lu^{cpx/opx}$ = 6) from this study. Two whole-rock Lu values were used: that for primitive mantle (Lu_{WR} = 0.0637 ppm; Hofmann, 1988) and 0.5 times primitive mantle. The initial and final modal abundances and the garnet-forming reaction are given in the caption to Figure 11, which shows the modeling results. The first garnet to nucleate in a primitive spinel lherzolite contains as much as 8 ppm Lu, but the Lu content decreases dramatically as more garnet is formed in the rock dropping four-fold to 2 ppm at ~2 wt.% garnet (Fig. 11). Lu abundances in pyroxenes decrease in concert with that of garnet assuming instant equilibration. Garnet in a primitive lherzolite with 12 wt.% garnet (a mode common for fertile Vitim lherzolites) should contain 0.5 ppm Lu (or 0.58 ppm Lu if the higher Lu_{PM} after Sun and McDonough (1989) is used).

Garnets from the majority of Vitim garnet lherzolites (average Lu 0.4–0.8 ppm; Figs. 4a and 6) plot close to the two model trends in Figure 11. None of those fertile peridotites have low modal garnet corresponding to high-Lu branches of the model trends at early stages of the spinel-to-garnet reaction. However, the latter are generally consistent with high Lu reported for garnet in peridotite xenoliths from Nushan (Fig. 4b), which have very low modal garnet (Xu et al., 2000). Furthermore, it is possible that core-rim garnet zoning (lower Lu in the rims) in some Vitim and Mongolian xenoliths is related to incomplete re-equilibration of the early (Lu-rich) and late-stage garnet during the spinel-to-garnet phase transition.

Lu-rich garnets in several Vitim xenoliths plot well above the trends calculated for garnets from primitive or moderately refractory peridotites (Fig. 11). The modal and major element data for those samples indicate that they were initially formed as partial melting residues, similar to Vitim peridotites with normal HREE levels. It follows that the Lu enrichments took place after the partial melting event. Furthermore, there is no evidence that metasomatism affected trace element patterns of those samples because their pyroxenes and garnet are depleted in LREE (Figs. 3 and 5). The only significant event in the postmelting history of the Vitim peridotite series appears to be the spinel-to-garnet phase transition, which is clearly indicated by the textural and other evidence (Ionov et al., 1993; Glaser et al., 1999; Ionov, 2004). Thus, it is natural to suggest that the HREE enrichments (or depletions) are related to the spinel-to-garnet transition, possibly due to HREE redistribution between adjacent domains of a modally heterogeneous peridotite series as first proposed by Ionov (2004).

After the partial melting episode, the Vitim peridotites were initially spinel facies rocks because garnet is not stable at depths <75 km at near-solidus temperatures; garnet formed in some peridotites during a later near-isobaric cooling. Experimentally determined phase equilibria (Nickel and Green, 1985; Robinson and Wood, 1998; Pearson et al., 2003) lead us to suggest that during the spinel-to-garnet phase transition, garnet initially nucleated in only the most fertile lherzolites. We argue that in some cases those garnet grains equilibrated with preexisting pyroxenes not only in their vicinity (on a mm scale), but also in more distant domains (on a cm-m scale) where local garnet nucleation had not yet occurred. The migration of HREE to the sites of early garnet nucleation was driven by the high affinity of HREE to garnet and produced bulk HREE enrichments in some fertile lherzolites and complementary HREE depletions in adjacent more refractory, garnet-free rocks (Ionov, 2004). Further garnet growth in the fertile rocks produced zoned garnets with lower HREE in the rims, whereas late-stage garnet nucleation in the more refractory rocks (which had lost some HREE) yielded heterogeneous, but generally HREE-poor garnets, which plot below the model trends in Figure 11, such as for sample 314-74.

The viability of this model hinges on two assumptions. The first one is that the lithospheric mantle beneath Vitim is chemically and modally heterogeneous on a cm-m scale so that fertile and more refractory peridotites are locally adjacent to each other. This assumption is generally supported by modal and chemical data on composite xenoliths from Vitim (Ionov et al.,1993; Ionov, 2004). Secondly, the model implies that some degree of limited chemical exchange in the lithospheric mantle is possible between rocks at distances greater than the size of largest modally homogeneous Vitim xenoliths (20–30 cm). Experimental data on REE diffusion rates indicate that such an exchange cannot be implemented by volume diffusion in minerals because it is too slow. For example, Van Orman et al. (2001) argue that significant Nd isotopic disequilibrium (differences in $^{143}Nd/^{144}Nd \geq 10^{-3}$) can be maintained for as long as ~1 Ga at 1150°C and 1.5 GPa between 5 mm clinopyroxene and garnet grains. Such estimates may vary depending on the choice of input parameters, like diffusion coefficients, grain size or definition of equilibrium. It is clear, however, that chemical exchange by diffusion at 1000 to 1100°C requires millions of years at distances of a few mm and is not efficient at larger scales (e.g., Bedini et al., 2004). The existence of HREE zoning in some central Asian garnets indicates that the volume diffusion failed to eliminate two-fold core-rim differences in Lu and Yb in mm-size grains. Importantly, the HREE zoning in the garnets cannot have been produced by diffusion-controlled REE fractionation because diffusion coefficients for all REE in pyrope garnet are similar (Van Orman et al., 2002a). It follows that the postulated HREE migration can only take place by intergranular exchange through grain boundaries. Experimentally determined Si grain boundary diffusion rate in forsterite aggregates is ~10^9 greater than the Si volume diffusion rate (Farver and Yund, 2000), indicating that diffusional transport of elements is dominated by

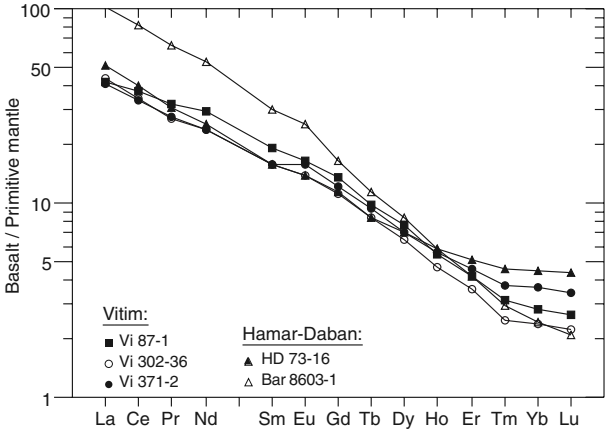

Fig. 12. Primitive mantle-normalized (Hofmann, 1988) REE abundances in basalts from the Baikal region: Vitim volcanic field (Ionov, 2004; Ionov et al., 2005) and Hamar-Daban range (Ionov et al., 1995; Ionov and Hofmann, 1995). Note big differences in HREE (but not necessarily in MREE-LREE) abundances of basalts from the same volcanic province.

grain boundaries. It is likely that the presence of very small amounts of stagnant interstitial fluid (e.g., filling triple grain junctions) could contribute to creating networks of high-diffusivity paths and thus further increase the transport rates.

One should note, however, that the interstitial chemical exchange over distances greater than several cm has a low capacity and could only concentrate certain trace elements in phases with very high partition coefficients for those elements (e.g., HREE and Sc in garnet; Rb, Ba and Nb in amphibole). We further emphasize that the above model does not involve regular, one-way fluid percolation (i.e., metasomatism), which very rapidly fractionates incompatible trace elements to create LREE enrichments and grain zoning (e.g., Ionov et al., 2002; Van Orman et al., 2002b) that have not been found in the Vitim xenoliths.

Altogether, we envisage the following sequence of events in the mantle source region of garnet-bearing xenoliths from the Vitim Miocene tuff (currently at a depth of 60–75 km). (1) A chemically heterogeneous peridotite series was produced by a major melting event at ~2 Ga, probably from a near-primitive asthenospheric source in the spinel stability field. (2) During the Caledonian orogeny and subsequent granitic magmatism the peridotites were spinel-facies rocks because ambient temperatures were >100°C higher than in early Miocene. (3) Slow isobaric cooling during the tectonic quiescence period from the middle Mesozoic to Miocene caused a gradual spinel-garnet phase transition, which first took place in more fertile rocks at a given depth. (3a) HREE migration to the sites of early garnet nucleation produced HREE-enriched peridotites at favorable conditions (proximity of garnet-free rocks, presence of interstitial fluids) as well as complementary HREE-depleted rocks. HREE-zoned garnets grew because of slow diffusion as temperatures dropped further. (4) Miocene basaltic volcanism induced local heating at the bottom of the lithospheric mantle and near magma conduits. The slow isobaric heating resulted in local breakdown of garnet to granular kelyphite matched by chemical zoning in pyroxene rims. (5) Peridotite fragments were randomly captured by host magma and transported to the surface at ~16 Ma; the rocks experienced short-term heating to magmatic temperatures and a pressure drop to form amorphous kelyphite.

6.6. Geodynamic Settings for Garnet-Controlled Chemical Fractionations and Inferences for HREE in Mantle-Derived Magmas

Isobaric cooling in the lithospheric mantle is not the only case when garnet-controlled HREE fractionation may take place. The spinel-to-garnet reaction imposed by rising ambient pressure is probably the first major phase transition following large-scale dehydration, which takes place in the down-going slab in subduction zones. Modal and major element heterogeneities in the slab (coexisting residual peridotites and oceanic crust) as well as the presence of interstitial fluids, favor heterogeneous garnet nucleation and ensuing HREE redistribution. The hypothetical HREE-rich (and complementary HREE-poor) components created in the subducted slab could be stored in the lower mantle or incorporated into the convecting asthenospheric mantle and contribute to Hf isotope variations in the sources of oceanic basalts.

The HREE migration may also take place during garnet-to-spinel facies transition, for example in a rising mantle diapir containing veins or blocks of garnet pyroxenite. As the ambient pressure in the rising diapir decreases, the host garnet peridotite will transform into a spinel lherzolite, but the pyroxenites will retain the garnet longer because of less refractory chemical compositions. At that stage, the garnet in the pyroxenites dispersed in spinel peridotites may scavenge some HREE from the adjacent peridotite to acquire humped, HREE-enriched patterns. When partial melting starts (or continues) in the rising diapir, the pyroxenites will melt sooner to yield magmas enriched in HREE. If such magma batches may reach the surface without significant re-equilibration with host peridotites, they could give rise to HREE-rich basalts. The same may apply to blocks of fertile garnet lherzolites embedded in refractory spinel peridotites. It is not likely that local HREE migration could produce large-scale mantle sources with distinct Lu/Hf. Nevertheless, rapid magma extraction and upward transport could probably yield distinct magma batches even from sources with small-scale (cm-m) HREE heterogeneities.

Basaltic series with broad variations in HREE abundances are common in intraplate volcanic fields including those in central Asia. Figure 12 shows REE patterns for selected basalts from two volcanic provinces in the Baikal region: Vitim and Hamar-Daban (Fig. 1). These samples have very similar MREE-LREE, but show a range of HREE abundances, with more than two-fold difference for Lu. Such differences in HREE are commonly seen as "garnet signature" implying that the source regions of the low-HREE magmas contain residual garnet (which effectively retains HREE) while the sources of the high-HREE magmas have no or little garnet. Our results could serve as a basis for an alternative hypothesis implying that the low- and high-HREE magmas may have been generated from sources with distinct HREE abundances. In such a case, the HREE-rich basalts may arise from selective melting of HREE-enriched garnet pyroxenite veins in spinel peridotites.

6.7. Inferences for Hf Isotope Variations in the Mantle and Mantle-Derived Magmas

Several earlier Lu-Hf isotope studies of mantle peridotites have yielded subsets of very high $^{176}Hf/^{177}Hf$ in clinopyroxene, garnet or whole-rocks, decoupled from Nd isotope compositions and plotting well above the mantle Hf-Nd array (Salters and Zindler, 1995; Schmidberger et al., 2002; Pearson et al., 2003; Bedini et al., 2004; Bizimis et al., 2004). This Hf-Nd isotope decoupling has been attributed to mixing of mantle sources with distinct Hf and Nd isotope compositions and/or to complex metasomatic processes in the mantle. The metasomatism is assumed to affect mainly Nd isotope compositions, but not so much Hf isotopes because of higher mobility of Nd relative to Hf in mantle fluids (Bedini et al., 2004; Bizimis et al., 2004).

Here, we propose an additional mechanism for creating mantle domains with high Lu/Hf and radiogenic Hf isotope compositions. We have shown that Lu-rich garnets and whole-rock peridotites (with Lu abundances and Lu/Hf higher than those in primitive mantle and partial melting residues) are common in the lithospheric mantle beneath central Asia, and possibly in off-craton lithospheric mantle worldwide. The high Lu/Hf in those rocks are not matched by correspondingly high Sm/Nd. Over time, they will develop radiogenic Hf isotope compositions, which will not be matched by equally radiogenic Nd isotope signatures. This phenomenon, probably related to Lu migration to the sites of early garnet nucleation during spinel-garnet phase transition, may be an

additional factor in creating Hf isotope heterogeneities in the upper mantle on a cm-meter scale. Similarly, Lu-depleted refractory peridotites (complementary to the Lu-enriched fertile rocks) could develop relatively unradiogenic Hf isotope compositions. Such rocks would plot below the mantle Hf-Nd array (assuming that the Lu-depletion is ancient and the Nd isotope compositions have not been affected by metasomatism). Unfortunately, none of the HREE-depleted Vitim peridotites have been analyzed for Hf isotopes. Finally, spinel peridotite series with decoupled Hf-Nd isotope compositions (like Hawaii; Bizimis et al., 2004) could have contained garnet lherzolites at an earlier stage of lithospheric history when the regional geotherm was colder and therefore garnet was stable in some fertile rocks. Overall, we argue that HREE redistribution during spinel-garnet phase transition after partial melting may be an important additional mechanism affecting HREE abundances, Lu/Hf values and Hf isotope compositions in mantle rocks.

Acknowledgments—DAI thanks I. Ashchepkov for help with fieldwork, M. Barfety and B. Moine for mineral separation, K.-P. Jochum, B. Stoll, K. Herwig and C. Hemond for help with LA-ICPMS analyses, J. de Jong and N. Mattielli for help with Hf isotope analyses, F. Albarède, A. Hofmann and J.Y. Cottin for assistance and advice. B. Boyer and C. Merlet provided SIMS analyses. Reviews of H. Becker, M. Bizimis and G. Pearson, and editorial comments of F. Frey have helped to improve the clarity of the manuscript. This research was supported by funding to DAI from Max-Planck-Institut für Chemie, Université Libre de Bruxelles, Russian Academy of Sciences and Australian Research Council. JBT acknowledges financial support from the French Institut National des Sciences de l'Univers. Part of this study in Brussels was funded by a FNRS grant (# 2.4607.01) to DW.

Associate editor: F. Frey

REFERENCES

Albarède F., Blichert-Toft J., Vervoort J. D., Gleason J. D. and Rosing M. (2000) Hf-Nd isotope evidence for a transient dynamic regime in the early terrestrial mantle. *Nature* **404,** 488–490.

Ashchepkov I. V. 1991) Deep-seated xenoliths of the Baikal rift. Nauka, Novosibirsk (in Russian).

Ashchepkov I. V. and André L. (2002) Pyroxenite xenoliths in picrite basalts (Vitim Plateau): origin and differentiation of mantle melts. *Russian Geol. Geophys.* **43,** 343–363.

Ashchepkov I. V., Dobretsov N. L. and Kalmanovich M. A. (1989) Garnet peridotite xenoliths from alkalic picritoid and basanitoid of the Vitim Plateau. *Trans. (Doklady) USSR Acad. Sci. Earth Sci. Sect.* **302,** 156–159.

Becker H. (1996) Crustal trace element and isotopic signatures in garnet pyroxenites from garnet peridotite massifs from Lower Austria. *J. Petrol.* **37,** 272–286.

Bedini R.-M. and Bodinier J.-L. (1999) Distribution of incompatible trace elements between the constituents of spinel peridotite xenoliths: ICP-MS data from the East African rift. *Geochim. Cosmochim. Acta* **63,** 3883–3900.

Bedini R.-M., Blichert-Toft J., Boyet M. and Albarède F. (2004) Isotopic constraints on the cooling of the continental lithosphere. *Earth Planet. Sci. Lett.* **223,** 99–111.

Bizimis M., Sen G. and Salters V. J. M. (2004) Hf-Nd isotope decoupling in the oceanic lithosphere: constraints from spinel peridotites from Oahu, Hawaii. *Earth Planet. Sci. Lett.* **217,** 43–58.

Blichert-Toft J. (2001) On the Lu-Hf isotope geochemistry of silicate rocks. *Geostand. Newsl.* **25,** 41–56.

Blichert-Toft J. and Albarède F. (1997) Lu-Hf isotope geochemistry of chondrites and the evolution of the mantle-crust system. *Earth Planet. Sci. Lett.* **148,** 243–258.

Blichert-Toft J., Chauvel C. and Albarède F. (1997) Separation of Hf and Lu for high-precision isotope analysis of rock samples by magnetic sector-multiple collector ICP-MS. *Contrib. Mineral. Petrol.* **127,** 248–260.

Blichert-Toft J., Ionov D. A. and Albarède F. (2000) The nature of the sub-continental lithospheric mantle: Hf isotope evidence from garnet peridotite xenoliths from Siberia. *J. Conf. Abstr.* **v. 5,** #217.

Bottazzi P., Ottolini L., Vannucci R. and Zanetti A. (1994) An accurate procedure for the quantification of rare earth elements in silicates. In *Secondary Ion Mass Spectrometry, SIMS IX* (eds. A. Benninghoven, Y. Nihei, R. Shimizu and H. V. Werner), pp. 927–930. Chichester: John Wiley.

Brey G. P. and Köhler T. (1990) Geothermobarometry in four-phase lherzolites II. New thermobarometers and practical assessment of existing thermobarometers. *J. Petrol.* **31,** 1353–1378.

Chauvel C. and Blichert-Toft J. (2001) A hafnium isotope and trace element perspective on melting of the depleted mantle. *Earth Planet. Sci. Lett.* **190,** 137–151.

Delvaux D., Moeys R., Stapel G., Melnikov A. and Ermikov V. (1995) Paleostress reconstructions and geodynamics of the Baikal region, Central Asia, Part I. Palaeozoic and Mesozoic pre-rift evolution. *Tectonophys.* **252,** 61–101.

Esin S. V., Ashchepkov I. V. and Ponomarchuk V. A. (1995) Petrogenesis of alkaline basaltoids from the Vitim plateau (Baikal rift zone). UIGGM SB RAS Press, Novosibirsk (in Russian).

Farver J. R. and Yund R. A. (2000) Silicon diffusion in forsterite aggregates: Implications for diffusion accommodated creep. *Geophys. Res. Lett.* **27,** 2337–2340.

Glaser S. M., Foley S. F. and Günther D. (1999) Trace element compositions of minerals in garnet and spinel peridotite xenoliths from the Vitim volcanic field, Transbaikalia, eastern Siberia. *Lithos* **48,** 263–285.

Green T. H., Blundy J. D., Adam J. and Yaxley G. M. (2000) SIMS determination of trace element partition coefficients between garnet, clinopyroxene and hydrous basaltic liquids at 2–7.7 GPa and 1080–1200°C. *Lithos* **53,** 165–187.

Hauri E. H., Wagner T. P. and Grove T. L. (1994) Experimental and natural partitioning of Th, U, Pb and other trace elements between garnet, clinopyroxene and basaltic melts. *Chem. Geol.* **117,** 149–166.

Hofmann A. W. (1988) Chem. differentiation of the Earth: the relationship between mantle, continental crust and oceanic crust. *Earth Planet. Sci. Lett.* **90,** 297–314.

Hofmann A. W. (2003) Sampling mantle heterogeneity through oceanic basalts: isotopes and trace elements. In *Treatise on Geochemistry. Vol. 2. The Mantle and Core* (ed. RW. Carlson), pp. 61–102. Elsevier.

Ionov D. (2002) Mantle structure and rifting processes in the Baikal-Mongolia region: geophysical data and evidence from xenoliths in volcanic rocks. *Tectonophys.* **351,** 41–60.

Ionov D. and Weis D. (2002) Hf-Nd-Sr isotope relationships in spinel and garnet facies peridotite xenoliths: inferences for the age and evolution of the lithospheric mantle. *Geochim. Cosmochim. Acta* **66,** A356 (abstr.).

Ionov D. A. (2004) Chemical variations in peridotite xenoliths from Vitim, Siberia: inferences for REE and Hf behaviour in the garnet facies upper mantle. *J. Petrol.* **45,** 343–367.

Ionov D. A., Ashchepkov I. V. and Jagoutz E. (2005) The provenance of fertile off-craton lithospheric mantle: Sr-Nd isotope and chemical composition of garnet and spinel peridotite xenoliths from Vitim, Siberia. *Chem. Geol.* **217,** 41–75.

Ionov D. A., Ashchepkov I. V., Stosch H.-G., Witt-Eickschen G. and Seck H. A. (1993) Garnet peridotite xenoliths from the Vitim volcanic field, Baikal region: the nature of the garnet-spinel peridotite transition zone in the continental mantle. *J. Petrol.* **34,** 1141–1175.

Ionov D. A., Bodinier J.-L., Mukasa S. B. and Zanetti A. (2002) Mechanisms and sources of mantle metasomatism: major and trace element compositions of peridotite xenoliths from Spitsbergen in the context of numerical modeling. *J. Petrol.* **43,** 2219–2259.

Ionov D. A., O'Reilly S. Y., and Ashchepkov I. V. (1995) Feldspar-bearing lherzolite xenoliths in alkali basalts from Hamar-Daban, Southern Baikal region, Russia. *Contrib. Mineral. Petrol.* **122,** 174–190.

Ionov D. A., Hofmann A. W. (1995) Nb-Ta-rich mantle amphiboles and micas: implications for subduction-related metasomatic trace element fractionations. *Earth Planet. Sci. Lett.* **131,** 341–356.

Ionov D. A. and Jagoutz E. (1988) Sr-Nd isotopic compositions in minerals of garnet and spinel peridotite xenoliths from the Vitim Plateau: first data on mantle inclusions from the USSR. *Doklady Academii Nauk SSSR* **301,** 1195–1198 (in Russian).

Jochum K. P., Dingwell D. B., Rocholl A., Stoll B., Hofmann A. W. et al. (2000) The preparation and preliminary characterisation of eight geological MPI-DING reference glasses for in-situ microanalysis. *Geostand. Newsl.* **24,** 87–133.

Johnson J. S., Gibson S. A., Thompson R. N., and Nowell G. M. (2005) Volcanism in the Vitim volcanic field, Siberia: Geochemical evidence for a mantle plume beneath the Baikal rift zone. *J. Petrol.* **46.** in press.

Johnson K. T. M. (1998) Experimental determination of partition coefficients for rare earth and high-field-strength elements between clinopyroxene, garnet and basaltic melt at high pressures. *Contrib. Mineral. Petrol.* **133,** 60–68.

Kempton P. D., Hawkesworth C. J., Lopez-Escobar L., Pearson D. G. and Ware A. J. (1999) Spinel ± garnet lherzolite xenoliths from Pali Aike, Part 2: Trace element and isotopic evidence on the evolution of lithospheric mantle beneath southern Patagonia. In *Proc. 7th Internatl. Kimberlite Conf.* (eds. J. J. Gurney, J. L. Gurney, M. D. S. Pascoe and H. Richardson), Vol. 1, pp. 415–428. RedRoof Design, Cape Town.

Kern H., Burlini L. and Ashchepkov I. V. (1996) Fabric-related seismic anisotropy in upper-mantle xenoliths: evidence from measurements and calculations. *Phys. Earth Planet. Inter.* **95,** 195–209.

Klemme S., Blundy J. D. and Wood B. J. (2002) Experimental constraints on major and trace element partitioning during partial melting of eclogite. *Geochim. Cosmochim. Acta* **66,** 3109–3123.

Kovalenko V. I., Ionov D. A., Yarmolyuk V., Jagoutz E., Lugmair G. W. and Stosch H.-G. (1991) Isotope data on the evolution of the mantle and its correlation with the evolution of the crust in some parts of central Asia. *Geochem. Internatl.* **28,** 82–92.

Litasov K. D., Foley S. F. and Litasov Y. D. (2000) Magmatic modification and metasomatism of the subcontinental mantle beneath the Vitim volcanic field (East Siberia): evidence from trace element data on pyroxenite and peridotite xenoliths from Miocene picrobasalt. *Lithos* **54,** 83–114.

Mocek B., Ionov D. and Boyd F. R. (2004) REE-partitioning between clinopyroxene and garnet in garnet-peridotite xenoliths: testing the lattice-strain model. *EGU* IA-05665 (abstr.).

Münker C., Weyer S., Scherer E. and Mezger K. (2001) Separation of high field strength elements (Nb, Ta, Zr, Hf) and Lu from rock samples for MC-ICPMS measurements. *Geochem. Geophys. Geosyst.* **2,** 10.1029/2001GC000183.

Nickel K. G. and Green D. H. (1985) Empirical geothermobarometry for garnet peridotites and implications for the nature of the lithosphere, kimberlites and diamonds. *Earth Planet. Sci. Lett.* **73,** 158–170.

Pearce N. J. G., Perkins W. T., Westgate J. A., Gorton M. P., Jackson S. E., Neal S. R. and Chenery S. P. (1997) A compilation of new and published major and trace element data for NIST SRM 610 and NIST SRM 612 glass reference materials. *Geostand. Newsl.* **21,** 115–144.

Pearson D. G., Canil D. and Shirey S. B. (2003) Mantle samples included in volcanic rocks: xenoliths and diamonds. In *Treatise on Geochemistry. Vol. 2. The Mantle and Core* (ed. RW. Carlson), pp. 171–276. Elsevier.

Pearson D. G., Irvine G. J., Ionov D. A., Boyd F. R. and Dreibus G. E. (2004) Re-Os isotope systematics and platinum group element fractionation during mantle melt extraction: a study of massif and xenolith peridotite suites. *Chem. Geol.* **208,** 29–59.

Pearson D. G. and Nowell G. M. (2002) The continental lithospheric mantle: characteristics and significance as a mantle reservoir. *Phil. Trans. R. Soc. A* **360,** 2383–2410.

Pearson D. G. and Nowell G. M. (2004) Re-Os and Lu-Hf isotope constraints on the origin and age of pyroxenites from the Beni Bousera peridotite massif: implications for mixed peridotite-pyroxenite mantle sources. *J. Petrol.* **45,** 439–455.

Petit C., Koulakov I. and Deverchère J. (1998) Velocity structure around the Baikal rift from teleseismic and local earthquake traveltimes and geodynamic implications. *Tectonophys.* **296,** 125–144.

Rasskazov S. V. (1994) Magmatism related to the Eastern Siberia rift system and the geodynamics. *Bull. Centres Rech. Explor.-Prod. Elf Aquit.* **18,** 437–452.

Robinson J. A. C. and Wood B. J. (1998) The depth of the spinel to garnet transition at the peridotite solidus. *Earth Planet. Sci. Lett.* **164,** 277–284.

Salnikova E. B., Kozakov I. K., Kotov A. B., Kröner A., Todt W., Bibikova E. V., Nutman A., Yakovleva S. Z. and Kovach V. P. (2001) Age of Palaeozoic granites and metamorphism in the Tuvino-Mongolian Massif of the Central Asian Mobile Belt: loss of a Precambrian microcontinent. *Precamb. Res.* **110,** 143–164.

Salters V. J. M. and Longhi J. (1999) Trace element partitioning during the initial stages of melting beneath mid-ocean ridges. *Earth Planet. Sci. Lett.* **166,** 15–30.

Salters V. J. M. and White W. M. (1998) Hf isotope constraints on mantle evolution. *Chem. Geol.* **145,** 447–460.

Salters V. J. M. and Zindler A. (1995) Extreme $^{176}Hf/^{177}Hf$ in the sub-oceanic mantle. *Earth Planet. Sci. Lett.* **129,** 13–30.

Schmidberger S. S., Simonetti A., Francis D. and Gariepy C. (2002) Probing Archean lithosphere using the Lu-Hf isotope systematics of peridotite xenoliths from Somerset Island kimberlites, Canada. *Earth Planet. Sci. Lett.* **197,** 245–259.

Sherman S. I., Dem'yanovich V. M. and Lysak S. V. (2004) Active faults, seismicity and recent fracturing in the lithosphere of the Baikal rift system. *Tectonophys.* **380,** 261–272.

Stern C. R., Kilian R., Olker B., Hauri E. H. and Kyser T. K. (1999) Evidence from mantle xenoliths for relatively thin (<100 km) continental lithosphere below the Phanerozoic crust of southernmost South America. *Lithos* **48,** 217–235.

Sun S. S. and McDonough W. F. (1989) Chem. and isotopic systematics of oceanic basalts: implications for mantle composition and processes. In *Magmatism in the Ocean Basins* (eds. AD. Saunders and MJ. Norry), pp. 313–345. Geol. Soc. London Spec. Publ. **42**.

Takazawa E., Frey F. A., Shimizu N. and Obata M. (2000) Whole rock compositional variations in an upper mantle peridotite (Horoman, Hokkaido, Japan): Are they consistent with a partial melting process. *Geochim. Cosmochim. Acta* **64,** 695–716.

Van Orman J. A., Grove T. L. and Shimizu N. (2001) Rare earth element diffusion in diopside: influence of temperature, pressure, and ionic radius and an elastic model for diffusion in silicates. *Contrib. Mineral. Petrol.* **141,** 687–703.

Van Orman J. A., Grove T. L., Shimizu N. and Layne G. D. (2002a) Rare earth element diffusion in a natural pyrope single crystal at 2.8 GPa. *Contrib. Mineral. Petrol.* **142,** 416–424.

Van Orman J. A., Grove T. L. and Shimizu N. (2002b) Diffusive fractionation of trace elements during production and transport of melt in Earth's upper mantle. *Earth Planet. Sci. Lett.* **198,** 93–112.

Vervoort J. D. and Blichert-Toft J. (1999) Evolution of the depleted mantle: Hf isotope evidence from juvenile rocks through time. *Geochim. Cosmochim. Acta* **63,** 533–556.

Walter M. J. (2003) Melt extraction and compositional variability in mantle lithosphere. In *Treatise on Geochemistry. Vol. 2. The Mantle and Core* (ed. RW. Carlson), pp. 363–394. Elsevier.

Wiechert U., Ionov D. A. and Wedepohl K. H. (1997) Spinel peridotite xenoliths from the Atsagin-Dush volcano, Dariganga lava plateau, Mongolia: A record of partial melting and cryptic metasomatism in the upper mantle. *Contrib. Mineral. Petrol.* **126,** 345–364.

Xu X., O'Reilly S. Y., Griffin W. L. and Zhou X. (2003) Enrichment of upper mantle peridotite: petrological, trace element and isotopic evidence in xenoliths from SE China. *Chem. Geol.* **198,** 163–188.

Xu X., O'Reilly S. Y., Griffin W. L. and Zhou X. (2000) Genesis of young lithospheric mantle in southeastern China: an LAM-ICPMS trace element study. *J. Petrol.* **41,** 111–148.

ELECTRONIC ANNEX

Supplementary data associated with this article can be found, in the online version, at doi: 10.1016/j.gca.2004.11.008.